Available online at www.sciencedirect.com
SCIENCE DIRECT®
ELSEVIER
International Journal of Multiphase Flow 31 (2005) 1063–1096
International Journal of Multiphase Flow
www.elsevier.com/locate/ijmulflow

Vertical stability of bubble chain: Multiscale approach

M.C. Ruzicka *

Institute of Chemical Process Fundamentals, Czech Academy of Sciences, Rozvojova 135, Prague 16502, Czech Republic

Received 11 November 2003; received in revised form 29 May 2005

Abstract

Linear stability is investigated of a uniform chain of equal spherical gas bubbles rising vertically in unbounded stagnant liquid at Reynolds number $Re = 50$–200 and bubble spacing $s > 2.6$ bubble radii. The equilibrium bubble positions are questioned for their stability with respect to small displacements in the vertical direction, parallel to the chain motion. The transverse displacements are not considered, and the chain is assumed to be laterally stable. The bubbles are subjected to three kinds of forces: buoyant, viscous, inviscid. The viscous and inviscid forces have both pairwise (local) and distant (nonlocal) components. The pairwise forces are expressed by the leading-order formulas known from the literature. The distant forces are expressed as a linear superposition of the pairwise forces taken over several farther neighbours. The stability problem is addressed on three different length scales corresponding to: discrete chain (microscale), continuous chain (mesoscale), bubbly chain flow (macroscale). The relevant governing equations are derived for each scale. The microscale equations are a set of ODE's, the Newton force laws for the individual discrete bubbles. The mesoscale equation is a PDE for bubbles continuously distributed along a line, obtained by taking the continuum limit of the microscale equations. The macroscale equations are two PDEs, the mass and momentum conservation equations, for an ensemble of noninteracting mesoscale chains rising in parallel. This transparent two-step process (micro → meso → macro) is an alternative to the usual one-step averaging, in obtaining the macroscale equations from microscale information. Here, the scale-up methodology is demonstrated for 1D motion of bubbles, but it can be used for behaviour of 2D and 3D lattices of bubbles, drops, and solids.

It is found that the uniform equilibrium spacing results from a balance between the attractive and repulsive forces. On all three length scales, the equilibrium is stabilized by the viscous drag force, and destabilized by the viscous shielding force (*shielding instability*). The inviscid forces are stability neutral and

* Tel.: +420 2 203 90299; fax: +420 2 209 20661.
E-mail address: ruzicka@icpf.cas.cz

0301-9322/$ - see front matter
doi:10.1016/j.ijmultiphaseflow.2005.05.011

generate conservative oscillations and concentration waves. The stability region in the parameter plane $s - Re$ is determined for each length scale. The stable region is relatively small on the microscale, larger on the mesoscale, and shrinks to zero on the macroscale where the bubbly chain flow is inherently unstable.

The *shielding instability* is expected to occur typically in intermediate Re flows where the vertical bubble interactions dominate over the horizontal interactions. This new kind of instability is studied here in a great detail, likely for the first time. Its relation to the elasticity properties of bubbly suspension on different length scales is discussed too. The shielding force takes the form of a negative bulk modulus of elasticity of the bubbly mixture.

Keywords: Bubble chain; Stability; Distant coupling; Multiscale; Shielding instability; Bulk elasticity

1. Introduction

One-dimensional arrays of interacting particles are of high interest, both on their own, and as a prelude to two and three spatial dimensions (Bernasconi and Schneider, 1981). The one-dimensionality usually makes the problem tractable or at least near-tractable (Mattis, 1993). This holds equally well for dispersed particles subjected to hydrodynamic forces. In-line interactions commonly occur in various flow situations, e.g. aerosols and atmospheric problems (Pruppacher and Klett, 1998), sprays and combustion (Sirignano, 1999), granular flows (Hinch and Saint-Jean, 1999), sedimentation (Happel and Brenner, 1965; Dixon et al., 1976), fluidized beds (Werther, 1977; Foscolo and Gibilaro, 1984; Broadhurst, 1986), and also in gas–liquid systems (e.g. Harper, 2001; Liger-Belair and Jeandet, 2002), which is the topic of the present study. The uniform bubble chain possesses the translational symmetry, where all particles are subjected to the same force law. Ideally, the chain is infinite. However, finiteness is needed both in calculations and measurements. Therefore, the fixed-end boundary condition is employed in modelling, and the continuous generation of bubbles in experiments. Both correspond to observing only a finite segment within a virtually infinite chain.

Continuously generated uniformly spaced bubble chains passing through finite layers of quiescent liquids do exist and have been observed in many experiments, in ranges of the Reynolds and other relevant numbers. This means that they are both vertically and laterally linearly stable; otherwise we could not produce them. The bubble formation process can be quite complicated in real systems, and sophisticated ways of bubble generation have to be used to control it. Usually, the bubble size and spontaneous formation frequency have been measured (Coppock and Meiklejohn, 1951) and coalescence phenomena studied (Nevers and Wu, 1971). Recently, acoustic emissions generated by a bubble chain has been investigated too (Manasseh et al., 2004). The chain speed is higher than the single bubble speed due to the collective drag reduction (e.g. Miyahara et al., 1984; Zhang and Fan, 2003). This so-called *shielding effect* is particularly strong at low bubble spacing, s less than 10, say. The shielding is typical for the strictly in-line arrangement where a bubble travels in the wake of the preceding bubble (local interaction), or, more generally, in the liquid disturbed by all preceding bubbles (distant interactions). The shielding effect is in a severe contrast with the *hindrance* effect that results in higher collective drag of bubbles rising in general positions, which is the usual case of real bubble suspensions (e.g. Richardson and Zaki, 1954), see Fig. 2.

Although bubble chains have been observed and studied for a long time, little attention has been paid to their vertical and lateral stability. Nevertheless, certain achievements have been reached. In the inviscid limit, the chain is *vertically* unstable (Harper, 1970; Galper and Miloh, 1998; Voinov, 2001). The only interaction force is the repulsive inertial force $\sim s^{-4} + \mathrm{O}(s^{-6})$ coming from the Bernoulli effect due to higher pressure between the bubbles. At high Re, small viscosity effects result in vertical stabilization. Harper (1970) develops an analytical theory based on the boundary layer approximation. The trailing bubble passes through the fluid that was in the boundary layer of the previous bubble and was given an upward velocity. The trailing drag is therefore lower. The drag difference is an attractive force that compensates for the inertial repulsion and produces a stable equilibrium. Because each bubble contributes to the velocity disturbance, the drag decreases along the line progressively, and the chain is more and more compressed due to the strong cumulative effect of all preceding bubbles. The viscous diffusion of the velocity disturbances between the bubbles is neglected, which has two important consequences: the theory applies only to short chains (actually only to a two-bubble chain–bubble pair), and, the trailing drag is independent of the bubble spacing, which is not true in reality. Harper (1997) improves the original theory by accounting for the vorticity diffusion in the bubble wake and obtains the trailing drag decreasing with decreasing bubble spacing. Except for low bubble spacing, his result is in a good quantitative agreement with the full numerical solution to the axisymmetric flow past a bubble pair calculated by Yuan and Prosperetti (1994) at intermediate $Re = 50$–200. Recently, a stable bubble pair in a similar range of Re has been found in experiments (Sanada, 2005). To the author's knowledge, there are no rigorous results for longer bubble chains at the moderate Re. The main drawback of the Harper's theory is the progressive drag reduction that excludes the uniform spacing and leads to increasing bubble velocity downchain. To keep the picture realistic, one must take into account the temporal viscous decay of the velocity disturbances created by the passing bubbles. If the disturbances decay quickly enough, the drag converges fast, and the front part of the chain with an uneven spacing is short. Disregarding this front part is equivalent to imposing the fixed-end boundary condition. Based on this reasoning, a simple force-law model is developed for dynamic behaviour of longer chains at $Re = 50$–200 (Ruzicka, 2000, referred to as R1). The formulas for the relevant pairwise forces at the leading order are taken from the literature and the unknown distant forces are modelled by the linear superposition of the local forces, because of lack of anything better. The model indicates a possibility for the chain vertically stability. At smaller $Re = 0.2$–35, it follows from experiments by Katz and Meneveau (1996), that the inertial repulsion is not strong enough to resist the viscous attraction and the bubbles coalesce. In the viscous limit, the chain is vertically unstable again. Here, the uniform spacing is not a result of a balance between attractive and repulsive forces, but merely reflects the fact that evenly spaced bubbles have the same drag and rise at the same speed, faster at low spacing (e.g. Sonshine and Brenner, 1966).

Since we are interested in strictly 1D problem (stability in vertical direction), the *lateral* chain stability is only briefly mentioned. Both the inviscid (Harper, 1970; Voinov, 2001) and viscous (Lerner and Harper, 1991) chains are laterally unstable, because there is no restoring force perpendicular to the direction of motion. Small viscosity does not stabilize the chain laterally (Harper, 1970). On the other hand, such a restoring force can be generated by an uneven distribution of a surfactant over the bubble surface (Harper, 1970; Lerner and Harper, 1991). At the intermediate Re, it seems that there are no rigorous results. A subtle point is the relation between the

lateral behaviour of a single bubble and bubble chain. The instability mechanism is likely different: the former requires a deformed bubble (presence of destabilizing force—shedding of vorticity from edges of larger curvature, two threads of opposite and alternating signs), while the latter occurs at a train of spherical bubbles (absence of stabilizing force). The bubble path instability (air in water) occurs for *Re* larger than 500–600, say (Magnaudet and Eames, 2000; Vries et al., 2002).

It follows that our knowledge on the chain stability at the *intermediate* Reynolds number is rather weak. This region is well beyond the power of analytical techniques, and we are on mercy of experiments, numerical simulations, and simple semi-empirical models. For instance, making a finite list of closed-form formulas for forces acting on a bubble is a common example of the last approach. If the list contains all relevant terms, and the formulas are correct at the leading order, it may be a success. There is an implicit hope that the results will also be leading-order correct. This approach is undertaken in R1, where a simple model for bubble chain is developed and some typical solutions are presented to illustrate the model ability and to support the modelling concept. Stemming from this model, the present study concerns the vertical stability of bubble chain on three different length scales. The study features the following aspects that have not been paid enough attention so far: (i) detailed analysis of chain vertical stability at moderate *Re*, (ii) phenomenon of shielding instability, (iii) effects of distant coupling between bubbles, both viscous and inviscid, (iv) multiscale approach and scale-up methodology, how to get from pairwise forces to macroscopic equations for bubbly mixtures, without averaging.

2. Physical model

The governing equations for the discrete chain were introduced and extensively discussed in R1, and only briefly are presented here. They apply to the microscale, Section 3.1, and are also used for deriving the equations for the larger scales in Sections 3.2 and 3.3.

Consider a one-dimensional array of N spherical nondeformable incompressible equal-sized gas bubbles of radius r arranged in a vertical line rising freely under buoyancy in an unbounded body of a quiescent liquid at a steady speed v with respect to the laboratory, Fig. 1a. Bubbles' positions are expressed by departures $y_i = x_i - x_{is}$ from their equilibrium positions x_{is} with uniform spacing d. The centre–centre distance between bubbles i and j is $d_{ij} = \mathrm{sign}(j-i)\cdot(y_j - y_i) + |j-i|d$ and the particular distance $d_{i,i+1}$ is denoted by d_i. Bubbles' velocities relative to the liquid are $v_i = v + \dot{y}_i$. After scaling by r and v, the dimensionless variables are:

$$u_i = y_i/r, \quad s = d/r, \quad s_{i,j} = d_{i,j}/r, \quad s_i = d_i/r, \quad \text{time} = t/(r/v), \quad \text{speed} = 1 + \dot{u}_i. \tag{2.1}$$

Three forces act on each bubble: buoyant, viscous, and inviscid (inertial, potential) forces. The latter two have both local and nonlocal components. The local force on bubble i comes from the nearest neighbours ($i \pm 1$) and the nonlocal force from the distant neighbours ($i \pm 2, 3, \ldots$). The bubbles are endowed with the added mass and the coefficient is taken 0.5 for all bubbles. This is sensible since in a uniform array all bubbles have the same coefficient and its value departs from 0.5 only at very low spacing, not considered here (e.g. Cai and Wallis, 1992; R1 p. 1155). The dimensionless forces are as follows. The buoyancy force applies to all bubbles:

$$B = 2gr/v^2. \tag{2.2}$$

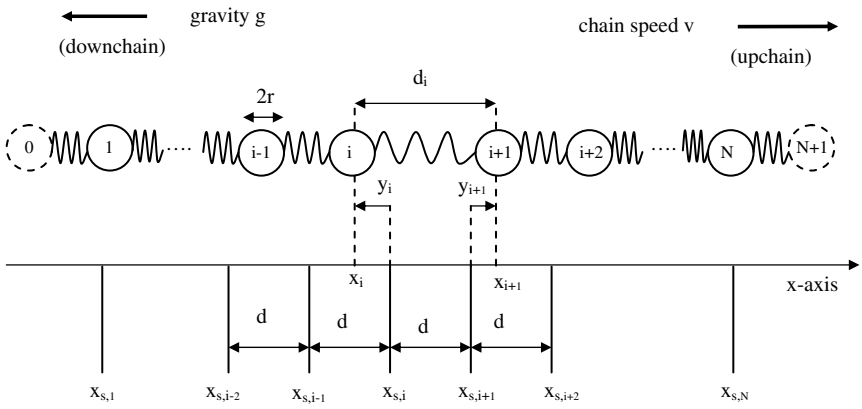

(a) Discrete chain: hydrodynamic mass-spring system

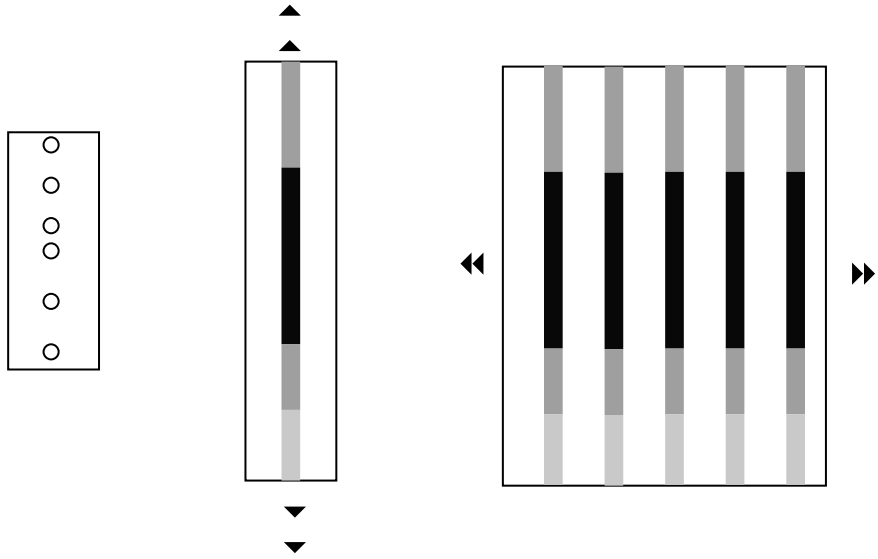

(b) Discrete chain (c) Continuous chain (d) Bubbly chain flow

Fig. 1. Bubble chain. (a) Definition sketch, (b) microscale: common bubble chain (mass–spring system), (c) mesoscale: bubbles continuously distributed along vertical line (one continuous string), and (d) macroscale: ensemble of continuous strings (bubbly chain flow).

The local viscous force on bubble i is the drag force

$$D_i = (3/4)(1 + \dot{u}_i)^2 C_i \tag{2.3}$$

with the local drag coefficient

$$C_i = (48/Re)(1 - F_i/Re^{0.5}) \tag{2.4}$$

and the Reynolds number $Re = 2rv_0/\eta$, where v_0 is the bubble terminal velocity and η, the liquid kinematic viscosity. The local drag factor is

$$F_i = 2.2 + 2.5(s_i - 2)^{-0.6}. \tag{2.5}$$

The constant term 2.2 belongs to an isolated bubble (Moore, 1963) and the distance-dependent term $2.5(s_i - 2)^{-0.6}$ is the additional drag reduction due to the shielding effect by the preceding bubble (Yuan and Prosperetti, 1994). Eq. (2.5) is valid for $s_i \geqslant 2.6$. D_i is a pairwise long-range attractive force $\sim s^{-0.6}$ caused by the wake suction. The distant viscous force is

$$V_i = (3/4)(1 + \dot{u}_i)^2 C_i^* \tag{2.6}$$

with the distant drag coefficient

$$C_i^* = 48\, Re^{-1.5} F_i^*. \tag{2.7}$$

The distant drag factor

$$F_i^* = \sum_{j=i+2}^{i+p+1} 2.5\alpha_j (s_{i,j} - 2)^{-0.6} \tag{2.8}$$

is taken as a linear superposition of the pairwise shieldings generated by p preceding distant neighbours $i+2, i+3, \ldots, i+(p+1)$. The scale-estimated damping factor

$$\alpha_j = \exp(-2s_{i,j}/Re) \tag{2.9}$$

accounts for the viscous dissipation of the disturbances introduced by the wakes of the preceding bubbles and ensures the convergence of (2.8) at $p \to \infty$.

The local inviscid force is (Lamb, 1932; Harper, 1970; Yuan and Prosperetti, 1994)

$$P_{i,i-1} = (3/4)(1 + \dot{u}_{i-1})^2 C_{i,i-1}, \tag{2.10}$$

$$P_{i,i+1} = (3/4)(1 + \dot{u}_{i+1})^2 C_{i,i+1} \tag{2.11}$$

with the symmetric force coefficient ($C_{i,j} = C_{j,i}$)

$$C_{i,j} = 12 s_{i,j}^{-4}, \tag{2.12}$$

which is independent of Re. It is a pairwise short-range repulsive force $\sim s^{-4}$ from the potential flow theory, generated by neighbours $i-1$ and $i+1$ on both sides. The distant inviscid force is taken as a linear superposition of the pairwise forces $P_{i,j}$ generated by q distant neighbours on both sides $i \pm 2, i \pm 3, \ldots, i \pm (q+1)$,

$$L_i = (3/4) \sum_{j=i-q-1}^{i-2} (1 + \dot{u}_j)^2 C_{i,j} \quad \text{(left neighbours in Fig.1a)}, \tag{2.13}$$

$$R_i = (3/4) \sum_{j=i+2}^{i+q+1} (1 + \dot{u}_j)^2 C_{i,j} \quad \text{(right neighbours in Fig.1a)}. \tag{2.14}$$

The subscripts i and j may be omitted at the quantities defined by (2.3)–(2.14) and these appear simply as $D, C, F, \ldots, C_p, L, R$.

The nonlinear dimensionless equations of motion of N individual bubbles in the chain read:

$$\ddot{u}_i = B + (3/4)(-D_i + P_{i,i-1} - P_{i,i+1} + hV_i + m(L_i - R_i)) \equiv f_i, \quad i = 1, 2, 3, \ldots, N. \tag{2.15}$$

These are the momentum equations written in deviations from uniformity, so that they apply to the reference frame fixed with both the chain and the laboratory, see Fig. 1a. The mass equation is trivial, $N =$ constant. The unknown relative strengths of the viscous and inviscid distant forces in (2.15) are expressed by h and m, both $\geqslant 0$. The chain is subjected to the fixed-end boundary condition, where identical bubbles with the same spacing are put to both ends of the N-chain, i.e. $u_i = \dot{u}_i = 0$ and $s_i = s$ for both $i < 1$ and $i > N$. This condition recovers the perfect translational symmetry of an infinite uniform array, because the end bubbles do not feel the boundaries. Since the stability concerns virtual motions near equilibrium, the condition does not matter. This condition can be applied to a continuously generated chain passing through a finite layer of liquid, or to an active 'window' of length N in a long chain.

The model has two main parameters, Reynolds number Re and steady bubble spacing s. Further parameters relate to the distant coupling. p and q are the numbers of viscous and inviscid distant neighbours considered and determine the spatial range of the nonlocal interactions. h and m are the weight factors of the viscous and inviscid distant forces and express the strength of the nonlocal forces relative to the local forces. Bubble radius r is used for the scaling and appears explicitly only in the buoyancy force (2.2), which does not affect the stability. N can also be considered as a parameter. The model is valid for $Re = 50$–200 and $s_i > 2.6$, where the drag formula (2.5) holds.

The nonlinear system (2.15) has an equilibrium solution of uniform steady spacing s and speed v, whose linear stability with respect to strictly 1D disturbances along the vertical (x-axis in Fig. 1a) is studied. Since the hydrodynamic forces depend on both the distances and velocities, each force gives two linear terms depending on either the distances (index d) or the velocities (index v). The linearized dimensionless equations (2.15) then read

$$\ddot{u}_i = (3/4)(D_d + D_v + P_d + P_v + h(V_d + V_v) + m(LR_d + LR_v)), \quad i = 1, 2, 3, \ldots, N, \tag{2.16}$$

where $(P_{i,i-1} - P_{i,i+1}) = P$ and $(L_i - R_i) = LR$ for brevity. The individual force terms are given by (3.1.3), (3.1.8) and (3.1.9).

The stability features of the force terms in (2.16) are investigated, both separately and in combinations. In the discrete case, the eigenvalues of the corresponding Jacobians are computed using the standard routines as implemented in *Mathematica 4.0* (Wolfram, 1999). The Jacobi matrix must be large enough to cover the whole coupling range. For local coupling, chain length is $N = 2$–10. For distant coupling, p, q are 1–3. In some cases, p is taken 1–6, to demonstrate the strong cumulative effect of the shielding. Most of the results are calculated with $h = m = 1$, which is considered as the maximum values of the weight factors. The purpose is to demonstrate the qualitative effect of the distant coupling on the chain stability. Therefore, only a limited selection of results is presented. The calculations show that the stability results are independent of N. It is therefore anticipated that they are valid also for longer chains. Physically, there is no apparent reason for the contrary: adding a bubble to the chain does not disturb the governing equations. Likely, we lack a theorem on the invariance of the spectrum with respect to the scale-up of a matrix of a given fixed pattern.

3. Results

3.1. Microscale: discrete bubble chain

The microscale model describes a chain of individual bubbles rising steadily at a uniform equilibrium spacing. These chains can be produced in laboratory and the results of this section can be verified experimentally, see Fig. 1b. The corresponding mechanical system is the classical mass–spring system, the archetype modelling concept for studying interactions in arrays of atoms and molecules.

The microscale governing equations for Section 3.1 are (2.15) and (2.16). Eq. (2.15) admits the equilibrium solution $u_i = \dot{u}_i = \ddot{u}_i = 0$, with steady speed v and uniform spacing s. The dimensional chain speed

$$v = \left(\frac{8gr}{3(C - hC^*)}\right)^{0.5} \tag{3.1.1}$$

is determined by the balance between the buoyant and viscous forces, because the inviscid forces cancel from (2.15) for the symmetry reason. The speed depends on r, s, Re and h. The speed obeys the single bubble formula where the collective chain drag $(C - hC^*)$ is always lower then the single bubble drag C_0. Also, the single bubble drag is lower than the drag of hindered rise of bubbles in general positions, see Fig. 2.

3.1.1. Nearest-neighbour approximation

If the distant effects are negligible $(h, m = 0)$, the force equation (2.16) reduces to

$$\ddot{u}_i = (3/4)(D_d + D_v + P_d + P_v) \quad (i = 1, 2, \ldots, N), \tag{3.1.2}$$

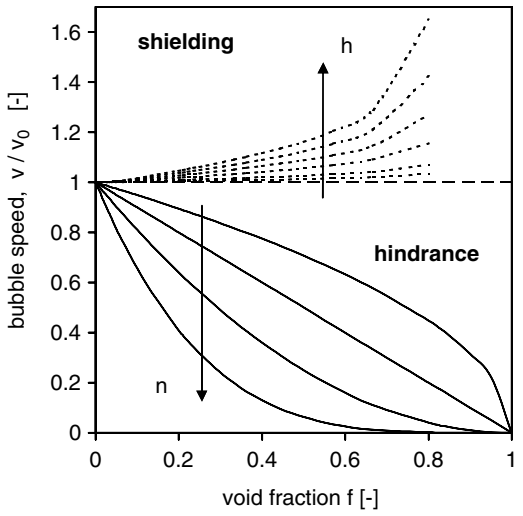

Fig. 2. Chain speed. Effect of bubble spacing s on collective bubble speed v/v_0. Dotted lines: shielding effect (in-line arrangement of bubbles), Eq. (3.1.1), $h = 0.1$, 0.2, 0.4, 0.6, 0.8, 1. Full lines: hindrance effect (bubbles in general positions), Richardson-Zaki equation $v/v_0 = (1 - \phi)^n$ with $n = 0.5$, 1, 2, 4. For bubble chains, n would be *negative* (see e.g. Sankaranaranayan et al., 2002).

where the four linear force components are:

$$\begin{aligned} D_d &= -C'(u_{i+1} - u_i) \quad \text{(viscous shielding)} \quad [-u_x] \\ D_v &= -2C\dot{u}_i \quad \text{(viscous drag)} \quad [-u_t] \\ P_d &= C'_p(u_{i+1} - 2u_i + u_{i-1}) \quad \text{(inviscid repulsion)} \quad [u_{xx}] \\ P_v &= -2C_p(\dot{u}_{i+1} - \dot{u}_{i-1}). \quad \text{(inviscid repulsion)} \quad [-u_{txx}]. \end{aligned} \tag{3.1.3}$$

The prime denotes the absolute value of the spatial derivative of the force coefficients C and C_p in the equilibrium. Only two of these hydrodynamic forces do have mechanical counterparts in the classical mass–spring system: D_v corresponds to the friction force and P_d to the elastic spring force (e.g. Main, 1984). The other two forces D_d and P_v are purely hydrodynamic. The drag force D_v is the only dissipative force. The other three are conservative. P_d and P_v are the potential forces, hence conservative by definition. The viscous shielding component D_d depends only on one spatial variable and is therefore conservative too (its closed-path integral equals zero). This may be surprising at a force of viscous origin. Anticipating the continuum limit, the continuous counterparts of the discrete forces are shown in brackets in (3.1.3).

3.1.1.1. Equilibrium stability. Each force component in (3.1.2) separately gives an equilibrium point with certain stability features. These features contribute to the stability of the full chain, see Table 1.

The shielding D_d is the main source of *instability* (unstable saddle), which leads to chain fragmentation and clustering via positive feed-back $\ddot{u}_i \sim \dot{u}_i$. This kind of instability caused by the shielding effect, peculiar to the in-line bubble interactions, is therefore called the *shielding instability*. The drag D_v is the sole source of *stability* (stable node), $\ddot{u}_i \sim -\dot{u}_i$. Both P_d and P_v are stability neutral (centre points) and generate conservative oscillations. The stability of the individual components is independent of s and Re.

At low Re, the chain is governed by the viscous force $\mathrm{Vis} = D_d + D_v$ with an unstable equilibrium due to D_d (unstable saddle), so that viscous chains split into fragments. At high Re, the chain is governed by the stability neutral inertial force $\mathrm{Pot} = P_d + P_v$ (centre point) and undergoes oscillations. The complete force in (3.1.2) gives two kinds of equilibria, depending on s and Re, see Fig. 3 (bold line). This is the main result of this section. At low s and high Re, the chain is stable and recovers the uniformity via damped oscillations (stable focus). At high s and low Re, the chain is unstable due to the shielding instability, and splits into fragments via oscillations with diverging amplitudes (unstable saddle-focus).

Note that while the existence of the equilibrium spacing results from a balance between the viscous attraction (D_d) and the inviscid repulsion (P_d and P_v), its stability results from a competition between two viscous forces: stabilizing drag term (D_v) and destabilizing shielding term (D_d). Although the equilibrium point is a property of a linear system, its character is determined by roots of the characteristic polynomial of the Jacobi matrix, which is a nonlinear procedure. Therefore, the character of the equilibrium of composed forces cannot be obtained by simply adding the characters of the equilibria of individual forces. Nevertheless, some features can be predicted. For instance, hydrodynamic arrays should be less stable than mechanical arrays, because they contain the unstable shielding force. For completeness, Table 1 shows the stability features also for combinations of forces without direct physical meaning.

Table 1
Discrete chain

		Local				Distant					
		Viscous		Inviscid		Viscous		Inviscid			
		1	2	3	4	5	6	7	8	9	10
Discrete chain											
Individual											
1	Term	D_d	D_v	P_d	P_v	V_d	V_v	LR_d	LR_v		
2	Equilib	S	N	C	C	S	N	C	C		
3	Stab	u	s	n	n	u	u	n	n		
Combined										Equilib	Stab
Local											
4	Vis	*	*							S	u
5	Pot			*	*					C	n
6	Dis	*		*						C/SF	n/u
7	Vel		*		*					F	s
8	Con	*		*	*					SF	u
9	Mec		*	*						F	s
10	Hyd	*			*					C/SF	n/u
11	Full	*	*	*	*					F/SF	s/u
Distant											
12	TVis	*	*			*	*			S	u
13	TPot			*	*			*	*	C	n
14	Tdis	*		*		*		*		C/SF	n/u
15	TVel		*		*		*		*	F	s/u
16	Full	*	*	*	*	*	*	*	*	F/SF	s/u
Continuous chain											
Coeff.An											
17	A_1	1				2					
18	A_2					1					
19	A_3		1				2				
20	A_4			1		3		2			
21	A_5					2		1			
22	A_6				1				2		
23	A_7								1		

Summary of stability results. Individual forces of (2.16) are listed in row 1; local terms in columns 1–4, distant terms in 5–8. Equilibrium type is specified in row 2, its stability in row 3. Combined forces are listed in rows 4–16, terms involved are indicated by stars. Equilibrium type is specified in column 9, its stability in 10. Link between discrete (2.16) and continuous (3.2.4) equations is shown in rows 17–23. Each force in row 1 generates one or more summands of $A_{n,k}$ in (A1). Numbers in rows 17–23 are ks. Legend: Equilibrium type: C—centre, F—focus, N—node, S—saddle, SF—saddle-focus, C/SF—either C or SF depending on s, Re. Stability: s—stable, u—unstable, n—neutrally stable, n/u—either n or u depending on values of s and Re.

3.1.1.2. Small oscillations. The main oscillatory force is the inertial force P_d and the bubble chain then reduces to the frictionless mechanical mass-spring system:

$$\ddot{u}_i = (3/4)P_d = \gamma(u_{i+1} - 2u_i + u_{i-1}), \quad \gamma = (3/4)C'_p = 36s^{-5}, \quad i = 1, 2, \ldots, N. \tag{3.1.4}$$

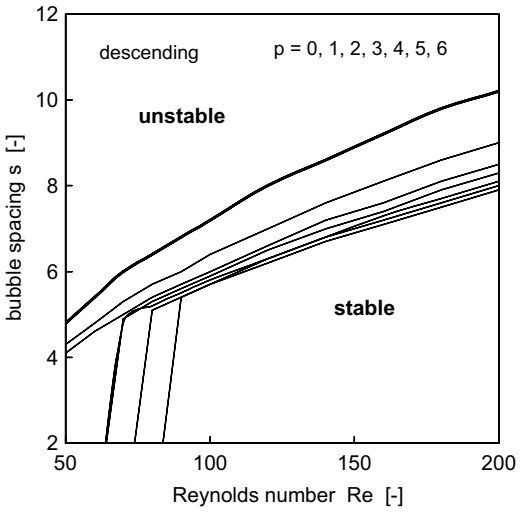

Fig. 3. Discrete chain. Stability diagram in parameter plane s–Re. Bold line ($s \approx 0.6\,Re^{0.54}$): local forces ($p = 0$). Thin lines: effect of increasing number p of viscous distant neighbours. Other parameters: $q = 3$, $h = 1$, $m = 1$ (bold line corresponds to Fig. 21 in R1).

The spring constant γ is the stiffness of a hypothetical hydrodynamic spring, and falls quickly with the equilibrium bubble pitch, $\sim s^{-5}$. The natural frequency of oscillations is $\omega_0 = \gamma^{0.5} = 6s^{-2.5}$. The spring modulus of elasticity is γs (Hirose and Lonngren, 1985). The linear system (3.1.4) can be decoupled into the normal modes. The normal modes of chains with 1–7 bubbles are calculated, see Fig. 4a and b and Table 2. The effect of the hydrodynamic shielding D_d on the mechanical oscillations can be seen from Figs. 4c and d and 5. The other oscillatory force is the inertial force P_v that gives similar oscillations like P_d. The full hydrodynamic array (3.1.2) cannot freely oscillate due to damping by D_v and destabilizing by D_d.

3.1.1.3. Discrete waves. Inserting wave solution $u_n(t) \sim \exp[\mathrm{i}(kns - \omega t)]$ into (3.1.4) gives dispersion relation and phase velocity:

$$\omega = \pm 2\omega_0 \sin(ks/2), \tag{3.1.5}$$

$$c = \omega/k = \pm(2\omega_0/k)\sin(ks/2). \tag{3.1.6}$$

Here, i is the imaginary unit; ns, the spatial coordinate; ω, the angular frequency; k, the wave number; λ, the wavelength, $k = 2\pi/\lambda$. The reflection at boundaries is not considered and (3.1.4) gives two wave modes with normal dispersion. The frequency falls to zero at $k_c = 2\pi/s$, where the discontinuity scale $\lambda_c = s$ is reached. For long waves, $k \to 0$, the discrete nature of the chain is irrelevant and the dispersion disappears, $\omega = \pm\omega_0 sk$ and $c = \omega_0 s = 6s^{-1.5}$. The other oscillatory force P_v, which is purely hydrodynamic, $\ddot{u}_i = -2C_p(\dot{u}_{i+1} - \dot{u}_{i-1})$, gives only one mode with normal dispersion moving upchain,

$$\omega = s\omega_0^2 \sin(ks) \tag{3.1.7}$$

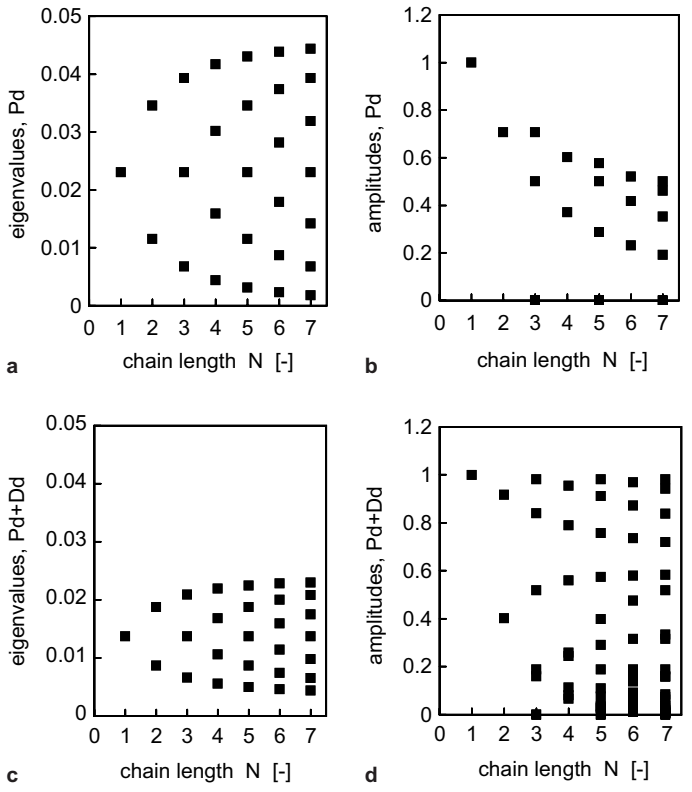

Fig. 4. Discrete chain. Effect of chain length N on normal modes. Elastic force, P_d: (a) squares of normal frequencies (eigenvalues), and (b) amplitudes of normal modes. The number of different amplitudes goes as $(N/2)$ for even N, and as $(3/2 + N/2)$ for odd N. Elastic + shielding force, $P_d + D_d$: (c) frequencies, and (d) amplitudes. Other parameters: $s = 5$, $Re = 100$.

Table 2
Discrete chain

Chain length N	1	2		3			4				5					6						7						
Mode no.	1	1	2	1	2	3	1	2	3	4	1	2	3	4	5	1	2	3	4	5	6	1	2	3	4	5	6	7
Bubble no.																												
1	+	+	+	+	+	+	+	+	+	+	+	+	+	+	+	+	+	+	+	+	+	+	+	+	+	+	+	+
2		–	+	–	0	+	–	–	+	+	–	–	0	+	+	–	–	–	+	+	+	–	–	–	0	+	+	+
3				+	–	+	+	–	–	+	+	0	–	0	+	+	+	–	–	+	+	+	+	–	–	–	+	+
4							–	+	–	+	–	+	0	–	+	–	+	+	–	–	+	–	0	+	0	–	0	+
5											+	–	+	–	+	+	–	+	+	–	+	+	–	–	+	–	–	+
6																–	+	–	+	–	+	–	+	–	0	+	–	+
7																						+	–	+	–	+	–	+

Phase structure of normal modes of chains with $N = 1$–7 bubbles generated by local elastic force P_d (+: in phase, −: out of phase).

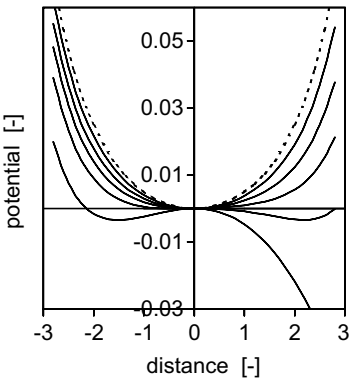

Fig. 5. Discrete chain. Potential well of bubble interactions in nearest-neighbour approximation. Dotted line: elastic force P_d. Full lines: effect of shielding force D_d (descending: $Re = 200, 120, 90, 70, 50$). Other parameters: $s = 6$.

with higher $\lambda_c = 2s$ and with the long-wave velocity $c = \omega_0^2 s^2 = 36 s^{-3}$. Thus, both inertial forces P_d and P_v can generate coherent motions in form of longitudinal concentration waves on scales $\lambda > \lambda_c$. The full hydrodynamic array (3.1.2) cannot support free waves due to presence of D_v and D_d.

3.1.2. Effect of distant coupling

The nearest-neighbour approximation may be bad when distant interactions come into play. Possible effects of the nonlocal coupling is investigated here. The importance of the distant forces is expressed in two ways: by the extent of the distant range (p and q), and by the relative strength of the distant coupling (h and m).

The viscous distant forces in (2.16) take the form

$$\begin{aligned} V_d &= -\sum_{n=2}^{p+1} C_n^{*\prime}(u_{i+n} - u_i) \quad [-u_{xx}, -u_{xxx}, \ldots, -u_{x\ldots x(p+1)\text{-times}}], \\ V_v &= 2C^* \dot{u}_i \quad [u_t], \end{aligned} \tag{3.1.8}$$

where the summation goes over p preceding distant neighbours and $C_n^{*\prime}$ is the absolute value of the spatial derivative of the nth summand in (2.7). The inviscid distant forces in (2.16) take the form

$$\begin{aligned} LR_d &= C_p' \sum_{n=2}^{q+1} (n)^{-5}(u_{i+n} - 2u_i + u_{i-n}) \quad [u_{xxxx}, u_{xxxxxx}, \ldots, u_{x\ldots x\ 2(q+1)\text{-times}}], \\ LR_v &= -2C_p \sum_{n=2}^{q+1} (n)^{-4}(\dot{u}_{i+n} - \dot{u}_{i-n}) \quad [-u_{txxxx}, -u_{txxxxxx}, \ldots, \ -u_{tx\ldots x\ 2(q+1)\text{-times}}], \end{aligned} \tag{3.1.9}$$

where the summation goes over q distant neighbours on both sides. While (3.1.8) presents a strong cumulative effect of the neighbours on the one side only, the contributions in (3.1.9) come from neighbours symmetrically placed on both sides and tend to cancel. Further, (3.1.9) falls quickly with both the spacing ($C_p \sim s^{-4}, C_p' \sim s^{-5}$) and the number of neighbours ($\sim n^{-4}$ and n^{-5}). It suggests that the viscous coupling could be more important than the inviscid one.

None of the four distant forces (3.1.8) and (3.1.9) has a mechanical analogue. Three of them are conservative (V_d, LR_d, LR_v) and one is antidissipative (V_v). V_v expresses the net drag reduction due to the distant coupling, which is equivalent to a negative viscosity coefficient ('antidrag'). In (2.16), hV_v must not be smaller than the local drag D_v to keep the model realistic, which gives a natural limit for h. In the continuum limit, the distant forces generate higher spatial derivatives that are of high physical importance: the distant forces are able to disperse waves. The viscous shielding V_d gives the forward derivatives up to the order $(p+1)$, first of which $-u_{xx}$ weakens the positive diffusion term $+u_{xx}$ produced by the local force P_d in (3.1.3). The inviscid repulsions LR_d and LR_v give the central derivatives up to the order $2(q+1)$. The higher derivatives can be interpreted as a tendency to long-range dynamic diffusion of bubbles ($u_{tt} \sim u_{xxxx}$) and bubble momentum ($u_{tt} \sim u_{txxxx}$).

3.1.2.1. Effect on stability, oscillations, and waves. Like the local shielding (D_d), also the distant shielding V_d destabilizes the chain (unstable saddle), see Table 1. However, unlike the local drag (D_v), the distant drag V_v destabilizes the chain (unstable node). Like the local inviscid forces (P_d and P_v), also the distant inviscid forces LR_d and LR_v are stability neutral (centre points). An important conclusions follows: none of the distant forces can contribute to the chain stability. The main result for the full chain is shown in Fig. 3 (thin lines). Due to the distant coupling, the stability region reduces. Especially, at low Re and strong coupling, no stable spacing exists and the chain splits into fragments inevitably. For completeness, the stability features of certain combinations of the local and distant forces are also shown in Table 1. It follows that the distant forces, either do not affect the stability features of the pairwise forces (TVis, TPot), or reduce the stability region (TDis), or destabilize the equilibrium (TVel). For instance, with the total velocity-related force, the stability created by the local part $D_v + P_v$ is destroyed by the distant part $hV_v + mLR_v$, see Fig. 6.

The inertial component LR_d has a weak effect on the oscillations produced by P_d. It slightly increases the normal frequencies, and splits the normal amplitudes that either coincide or are zero into slightly larger and smaller ones, so that the bubbles originally at rest start to move slightly. It does not affect the modal structure in Table 2. The shielding component V_d acts like its local coun-

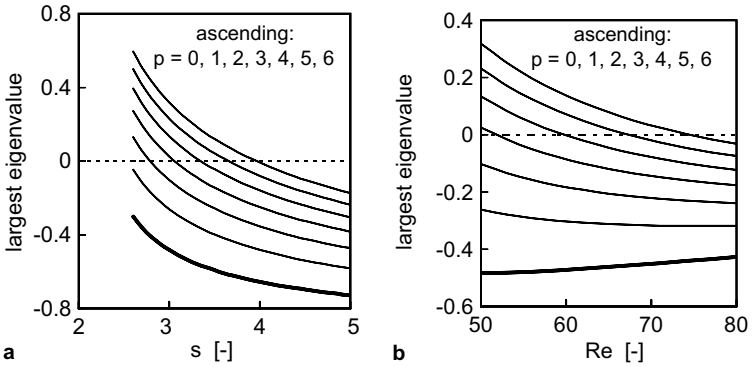

Fig. 6. Discrete chain. Destabilizing effect of increasing number of viscous distant neighbours p: largest eigenvalue becomes positive. Other parameters: (a) $Re = 50$, $q = 3$, $h = 1$, $m = 1$; and (b) $s = 3$, $q = 3$, $h = 1$, $m = 1$.

terpart D_d and tends to destroy of oscillations by additional deformation of the potential well in Fig. 5.

The forces LR_d and LR_v produce waves with the dispersion relations

$$\begin{aligned}&\text{Term } mLR_d : \omega^2 = 4m\omega_0^2 \sum_{n=2}^{q+1} n^{-5}\sin^2(nks/2) \quad \text{(two modes)},\\ &\text{Term } mLR_v : \omega = ms\omega_0^2 \sum_{n=2}^{q+1} n^{-4}\sin(nks) \quad \text{(one mode)},\end{aligned} \tag{3.1.10}$$

cf. 3.1.5,3.1.6,3.1.7. The discontinuity scale increases with the extent q of the nonlocal range like $\lambda_c = (q+1)s$ and $2(q+1)s$ respectively. The long waves ($k \to 0$) are dispersionless and move with velocities $c^2 = m\omega_0^2 s^2 \sum n^{-3}$ and $c = m\omega_0^2 s^2 \sum n^{-3}$ respectively. V_d acts like D_d. The distant drag V_v alone causes unphysical explosion of waves, but in combination with its local counterpart D_v, it only reduces the dissipation.

3.1.2.2. Coupling strength. There is a natural limit on the viscous coupling given by the denominator of (3.1.1), $h < C/C^*$. For the strongest possible interaction (low s, low Re, infinite p), we obtain $h < 0.34$, which is somewhat lower than an estimate 0.44 obtained on different grounds previously in R1. The inviscid coupling is supposed to be $m < 1$, because unity corresponds to a plain superposition of the pairwise forces. These should be weakened by bubbles placed in between, as there is no reason to think the opposite. Values of h and m can be obtained from experiments: h by measuring the steady chain speed given by (3.1.1), and m by measuring the oscillation frequency and the wave speed.

3.2. Mesoscale: continuous bubble chain

When an observer is sufficiently far from a long chain, its discrete nature (length scales $\sim r, s$) cannot be resolved and one sees bubbles *smoothly distributed* along a line, Fig. 1c. Such a 'coarse-grained' look represents a new modelling concept. This concept applies when the disturbance wavelength is much larger than the discrete length scale.

The step from the discrete to the continuous is facilitated by taking the continuum limit. It consists in replacing the discrete positions and velocities of the individual bubbles in (2.16) with their continuous counterparts, which are given by a smooth function $u(x,t)$ and its derivatives:

$$\begin{aligned}u_{i\pm n} &= u + u_x(\pm ns)^1 + (1/2!)u_{xx}(\pm ns)^2 + (1/3!)u_{xxx}(\pm ns)^3 \ldots, \quad n = 0,1,2,\ldots,\\ u_{i\pm n} &= u_t + u_{tx}(\pm ns)^1 + (1/2!)u_{txx}(\pm ns)^2 + (1/3!)u_{txxx}(\pm s)^3 \ldots\end{aligned} \tag{3.2.1}$$

These expansions may *formally* be of any length, but not all the terms can *physically* be justified. For instance, if higher spatial derivatives producing interesting effects in models are artefacts of insufficient truncation, these will not be detected in experiments because of absence of corresponding physical mechanisms. Therefore, only physically relevant terms are retained here, those indicated in brackets in (3.1.3), (3.1.8) and (3.1.9) for given p and q. To illustrate the effect of distant forces on the chain behaviour, four neighbours on both sides are considered, i.e. $p = q = 3$.

Substituting (3.2.1) into (3.1.3), (3.1.8) and (3.1.9) gives the continuous counterparts of the local discrete forces,

$$\begin{aligned} D_d &= -sC'u_x, \\ D_v &= -2Cu_t, \\ P_d &= s^2C'_p u_{xx}, \\ P_v &= -4sC_p u_{tx}, \end{aligned} \tag{3.2.2}$$

and the distant discrete forces,

$$\begin{aligned} V_d &= -s(2C_2^{*\prime} + 3C_3^{*\prime} + 4C_4^{*\prime})u_x - s^2(2C_2^{*\prime} + 4.5C_3^{*\prime} + 8C_4^{*\prime})u_{xx} - s^3(4.5C_3^{*\prime} + 10.6C_4^{*\prime})u_{xxx} - 10.6s^4C_4^{*\prime}u_{xxxx}, \\ V_v &= 2C^* u_t, \\ LR_d &= 0.177s^2C'_p u_{xx} + 0.09s^4C'_p u_{xxxx}[+0.019s^6C'_p U_{xxxxxx} + 0.003s^8C'_p u_{xxxxxxxx}], \\ LR_v &= -0.71sC_p u_{tx} - 0.722s^3C_p u_{txxx}[-0.233s^5C_p u_{txxxxx} - 0.05s^7C_p u_{txxxxxxx}]. \end{aligned} \tag{3.2.3}$$

The forces must decrease with increasing s, since the interactions must fall with distance. V_d converges at large s, so all terms can be retained in (3.2.3), of which u_{xxx} is the leading-order viscous distant term. LR_d and LR_v go like $\sim s^{-3} + s^{-1} + s^1 + s^3$, where only the first two terms can be retained. This is sensible, since the term s^{-1} is the last converging at large s and the first generated exclusively by the distant coupling. Therefore, u_{xxxx} and u_{txxx} are taken as the leading-order inviscid distant terms. Putting (3.2.2) and (3.2.3) at the leading order into (2.16) gives the mesoscale dimensionless momentum equation for small departures from the uniformity of bubbles continuously distributed along an infinite line:

$$u_{tt} = -A_1u_x - A_2u_{xxx} - A_3u_t + A_4u_{xx} + A_5u_{xxxx} - A_6u_{tx} - A_7u_{txxx}. \tag{3.2.4}$$

Since it is written in deviations, it applies to the reference frame fixed with both the chain and the laboratory. In mechanics, the continuum limit brings us from a discrete atomic array to the wave equation for a macroscopic material string. Therefore, (3.2.4) is the 'hydrodynamic' wave equation. Wave behaviour depends on both forces and geometry. Since we are interested in forces, we consider the simplest possible geometry—an infinite string without boundaries. Near the basic state (small motions within $s \pm u$), the thickness δ of the hypothetical string (whatever it is, usually not specified in this case), remains constant, $\delta =$ const., since the transversal deformation is negligible due to the infinitesimality of u. Then, the mesoscale mass equation is trivial, $s =$ const.

Unlike the discrete chain, the continuous chain does not directly refer to reality. It is a useful abstract concept that provides valuable insight into dynamics of large-scale disturbances in a medium whose 'subgrid details' are unresolved. In mechanics, the step from atoms to continuous wave equation spans over many orders of magnitude, and both concepts work well. Likely, the minimum step size for the matter forget its discrete nature is much smaller. This size, if known, indicates the necessary length-scale for the continuous models be realistic and experimentally verifiable. For this reason, the stability analysis of the mesoscale model is presented in Appendix A. On the other hand, the mesoscale concept is crucial for this study, since it serves as a bridge between micro- and macro-scales. The link micro–meso is indicated in Table 1, and that between meso and macro is shown in Table 3.

Table 3
Continuous chain

	A_1	A_2	A_3	A_4	A_5	A_6	A_7	
Continuous chain								
Term	$-u_x$	$-u_{xxx}$	$-u_t$	u_{xx}	u_{xxx}	$-u_{tx}$	$-u_{txxx}$	1
Stability	u	u	s	n/u	u/n	n	n	2
Viscous	1,2	1	1,2	3	2			3
Potential				1,2	1	1,2	1	4
Local	1		1	1		1		5
Distant	2	1	2	2,3	1,2	2	1	6
Bubbly chain flow								
Term	ϕ_x	ϕ_{xxx}	$-w$	$-\phi_{xx}$	$-\phi_{xxx}$	$-w_x$	$-w_{xxx}$	7

Summary of stability results. Seven force terms of Eq. (3.2.4) with coefficients A_{1-7} shown in Eq. (A1) are listed in row 1, their stability in row 2. Rows 3–6 show origin of summands $A_{n,k}$, numbers are ks. Link between continuous (3.2.4) and bubbly chain flow (3.3.4) equations is via comparing rows 1 and 7. Legend. Stability: s—stable, u—unstable, n—neutrally stable, n/u—either n or u depending on values of s and Re.

3.3. Macroscale: bubbly chain flow

3.3.1. Governing equations

To assess possible relevance of the in-line interactions for bubbly flows, consider a situation when an observer looking at a continuous chain from Section 3.2 expands the view sidewise and sees an *ensemble* of identical noninteracting chains, rising in parallel, see Fig. 1d. This is called 1D 'bubbly chain flow', where the vertical interactions dominate over the horizontal ones. Neglecting the lateral forces implies absence of a horizontal length-scale. The transverse extent of the system enables to consider the cross-section area (put to unity) and the mass flux through it, hence a nontrivial mass equation. The corresponding mechanical problem is a homogeneous isotropic material body with longitudinal waves propagating in one spatial direction.

The bubble concentration ϕ is here introduced as the linear void fraction,

$$\phi(x,t) \equiv 2/(s+u(x,t)). \tag{3.3.1}$$

The formula complies with the one-dimensional character of this study where bubbles are line segments and ϕ is the ratio (bubble size, $2r$)/(bubble spacing $(s+u)r$). For touching bubbles ($s=2, u=0$), $\varphi=1$, and for separated bubbles ($s\to\infty$), $\varphi=0$. With infinitesimal u, neither $s+u<2$ nor even <0 can occur. Note that the concentration can also be defined as the true 3D volumetric void fraction $(4/3)\pi/(s+u)s^2$, where the bubble volume is related to an elementary cubic cell. Both definitions differ only by a numerical factor $(2/3)\pi/s^2$. The following mass equation applies to 1D bubbly chain flow

$$\phi_t + [V\phi]_x = 0 \quad \text{(mass)}, \tag{3.3.2}$$

which is the dimensionless continuity equation. The bubble velocity $V(x,t)$ has two components, $V=U+w$. The equilibrium chain speed U relative to the laboratory is v given by (3.1.1) and scaled by v itself, thence $U=1$. In the reference frame fixed with the chain, $U=0$. The concentration disturbance speed w relative to the chain is identified with u_t, i.e. $w\equiv u_t$. Both v and w depend on ϕ. In the equilibrium, $u=0$, and (3.3.1) gives $\phi_0=2/s$, which after putting into (3.1.1)

gives the dependence $v(\phi_0)$. The dependence $w(\phi)$ is not known and must be found with help of the momentum equation. The linear version of (3.3.2) for small departures (ϕ and w) from uniformity (ϕ_0 and U) reads

$$\phi_t + U\phi_x + \phi_0 w_x = 0 \quad \text{(mass)}. \tag{3.3.3}$$

The mesoscale momentum equation (3.2.4) must be written in concentrations. Using (3.3.1) as the link between u and ϕ and their derivatives, (3.2.4) becomes:

$$w_t = aA_1\phi_x + aA_2\phi_{xxx} - A_3 w - aA_4\phi_{xx} - aA_5\phi_{xxxx} - A_6 w_x - A_7 w_{xxx} \quad \text{(momentum)}, \tag{3.3.4}$$

where $a = 2/\phi_0^2$. Eqs. (3.3.3) and (3.3.4) are the macroscale governing equations. Since we are interested in forces and not in geometry, an infinite medium is considered, and no boundary conditions employed. Inserting the wave solution $\sim\exp[\mathrm{i}(kx - \omega t)]$ into the governing equations gives the dispersion relation. The system either recovers the uniformity by damping the wavy disturbances (stability), or oscillates freely (neutral stability), or breaks the uniformity (instability). Allowing for the complex frequency to explore the temporal instability, $\omega = \omega_r + \mathrm{i}\omega_i$, the factor $\sim\exp(\omega_i t)$ stands at the amplitude of the solution and the sign of the imaginary part ω_i determines the stability (−stable, +unstable). Both ω_r and ω_i must be real. The sign of ω_r indicates the direction of the wave propagation (+: upchain, −: downchain).

3.3.2. Kinematic waves

When the viscous forces dominate, (3.3.4) reduces to

$$0 = aA_1\phi_x + aA_2\phi_{xxx} - A_3 w + aA_{4,3}\phi_{xx} + aA_{5,2}\phi_{xxxx} \quad \text{(momentum)}. \tag{3.3.5}$$

We want to express the disturbance speed w from (3.3.5), find w_x, and substitute it into (3.3.3): the expression

$$w = B_1\phi_x + B_2\phi_{xxx} + B_3\phi_{xx} + B_4\phi_{xxxx} \quad \text{(momentum)} \tag{3.3.6}$$

contains the essence of the near-equilibrium dynamics. The positive Bs are: $B_1 = aA_1/A_3$, $B_2 = aA_2/A_3$, $B_3 = aA_{4,3}/A_3$, $B_4 = aA_{5,2}/A_3$. Expressing formally the derivative w_x of (3.3.6) and putting into (3.3.3) gives the kinematic equation of small motions in terms of ϕ,

$$\phi_t + U\phi_x + \phi_0(B_1\phi_{xx} + B_2\phi_{xxxx} + B_3\phi_{xxx} + B_4\phi_{xxxxx}) = 0 \quad \text{(mass + momentum)}. \tag{3.3.7}$$

The dispersion relation of (3.3.7) reads

$$-\omega i + Uki + \phi_0(-B_1k^2 + B_2k^4 - B_3k^3 i + B_4k^5 i) = 0 \tag{3.3.8}$$

and gives

$$\begin{aligned} \omega_r &= Uk - \phi_0 B_3 k^3 + \phi_0 B_4 k^5, \\ \omega_i &= \phi_0 B_1 k^2 - \phi_0 B_2 k^4. \end{aligned} \tag{3.3.9}$$

In the nearest-neighbour approximation, (3.3.7) becomes

$$\phi_t + U\phi_x = -\phi_0 B_{1,1}\phi_{xx} \quad \text{(mass + momentum)}, \tag{3.3.10}$$

where the minus sign on the r.h.s. is significant, because it makes the equation 'antidiffusive'. The dispersion relation (3.3.9) then reduces to

$$\begin{aligned}\omega_r &= Uk,\\ \omega_i &= \phi_0 B_{1,1} k^2\end{aligned} \tag{3.3.11}$$

and yields an exponentially growing factor $\sim\exp(\phi_0 B_{1,1} k^2 t)$ at the wave mode $\exp[\mathrm{i}(kx - Ukt)]$ moving upchain at speed U. An important conclusion follows: the flow with local interactions is inherently unstable and cannot support kinematic waves. The instability is caused by the local shielding force. Indeed, the coefficient $B_{1,1} \sim A_{1,1}/A_3 \sim D_d/D_v \sim$ (local shielding)/(drag).

The effect of the distant forces follows from (3.3.9). The term B_3 causes the normal while the term B_4 the anomalous dispersion of waves. Both these are generated by the distant coupling. In ω_i, the destabilizing effect of $B_1 \sim$ (local + distant shielding) is suppressed by $B_2 \sim$ (distant shielding). An unexpected result arrives: the distant coupling plays a dual role and *can stabilize* the flow by damping concentration waves. The first term in ω_i dominates at long waves (small $k, k \leqslant k_{\max}$ set to 1) and low spacing, while the second at short waves and larger spacing (compare A_1 and A_2 in (3.3.5)).

3.3.3. Dynamic waves

When the inviscid forces dominate, (3.3.4) reduces to

$$w_t = -aA_{4,1+2}\phi_{xx} - aA_5\phi_{xxxx} - A_6 w_x - A_7 w_{xxx} \quad \text{(momentum)}. \tag{3.3.12}$$

As before, we want to merge the mass and momentum equations. For simplicity, the reference frame fixed with the chain is considered ($U = 0$ and $V = w$), where (3.3.3) reads

$$\phi_t = -\phi_0 w_x \quad \text{(mass)}. \tag{3.3.13}$$

Taking $\partial/\partial t$ of (3.3.12) and several $\partial/\partial x$ of (3.3.13) enables to eliminate ϕ from (3.3.12), and gives the dynamic equation of small motions in terms of w,

$$w_{tt} = a\phi_0 A_{4,1+2} w_{xxx} + a\phi_0 A_{5,1} w_{xxxxx} - A_6 w_{tx} - A_7 w_{txxx} \quad \text{(momentum + mass)}. \tag{3.3.14}$$

The dispersion relation of (3.3.14) reads

$$-\omega^2 = -a\phi_0 A_{4,1+2} k^3 i + a\phi_0 A_{5,1} k^5 i - A_6 \omega k + A_7 \omega k^3 \tag{3.3.15}$$

and gives for the imaginary part

$$b_0 + b_2\omega_i^2 + b_4\omega_i^4 = 0, \tag{3.3.16}$$

where the coefficients are

$$\begin{aligned} b_0 &= (a\phi_0)^2(-A_{4,1+2}^2 k^6 + 2A_{4,1+2}A_{5,1}k^8 - A_{5,1}^2 k^{10}),\\ b_2 &= A_6^2 k^2 - 2A_6 A_7 k^4 + A_7^2 k^6,\\ b_4 &= 4. \end{aligned} \tag{3.3.17}$$

Consequently, the typically nonzero solution

$$\omega_i = \pm[(1/8)(-b_2 \pm (b_2^2 - 16b_0)^{1/2})]^{1/2} \tag{3.3.18}$$

generates both damping and growing factors in the wave, so that the uniform state is not stable. Long dynamic waves can propagate freely, since at $k \to 0$ also ω_i turns to zero. The

nearest- neighbour approximation does not bring any notable simplification to (3.3.18), and gives the same result.

3.3.4. Stability of bubbly chain flow

The kinematic and dynamic modes are the two limiting cases. Here, the stability of the uniform bubbly chain flow is investigated, where both the viscous and inviscid forces are considered. Small disturbances to the homogeneous state may be resolved into independent Fourier modes,

$$\phi = \Phi \exp[\mathrm{i}k(x - ct)], \quad w = W \exp[\mathrm{i}k(x - ct)], \tag{3.3.19}$$

where the wave number k is real but the phase speed c is complex. Putting (3.3.19) into (3.3.3) moving with the chain ($U = 0$), and into (3.3.4), gives two equations for the amplitudes Φ and W,

$$\begin{aligned} &(-\mathrm{i}kc)\Phi + (\mathrm{i}k\phi_0)W = 0, \\ &[\mathrm{i}ka(A_1 - k^2A_2) + k^2a(A_4 - k^2A_5)]\Phi + [\mathrm{i}k(c - A_6 + k^2A_7) - A_3]W = 0. \end{aligned} \tag{3.3.20}$$

The condition for existence of a nonzero solution of (3.3.20) is the zeroness of the determinant. It gives the quadratic equation for the growth factor c,

$$c^2 + (k_1 + \mathrm{i}k_2)c + (k_3 + \mathrm{i}k_4) = 0 \tag{3.3.21}$$

with the solution

$$c = (1/2)[-(k_1 + \mathrm{i}k_2) \pm \{(k_1 + \mathrm{i}k_2)^2 - 4(k_3 + \mathrm{i}k_4)\}^{1/2}] \tag{3.3.22}$$

or, equivalently,

$$c = (1/2)\left[-k_1 - \mathrm{i}k_2 \pm \sqrt{k_5 + \mathrm{i}k_6}\right] \tag{3.3.23}$$

with the real and imaginary parts

$$\begin{aligned} c_r &= (1/2)\left[-k_1 \pm \sqrt{1/2}\ ((k_5^2 + k_6^2)^{1/2} + k_5)^{1/2}\right], \\ c_i &= (1/2)\left[-k_2 \pm \sqrt{1/2}\ ((k_5^2 + k_6^2)^{1/2} - k_5)^{1/2}\right] \end{aligned} \tag{3.3.24}$$

using the following notation:

$$\begin{aligned} &k_1 = -A_6 + k^2A_7, \quad k_2 = A_3/k, \quad k_3 = a\phi_0(A_1 - k^2A_2), \quad k_4 = -a\phi_0k(A_4 + k^2A_5), \\ &k_5 = k_1^2 - k_2^2 - 4k_3, \quad k_6 = 2k_1k_2 - 4k_4. \end{aligned} \tag{3.3.25}$$

The uniform state is stable if

$$c_i(k, s, Re, h, m) < 0. \tag{3.3.26}$$

In (3.3.24), the root c_i with the minus sign is always negative and gives a stable solution. The other root with the plus sign can be either negative or positive, and is therefore relevant for the stability. The root is typically positive, and rarely it takes negative values for a limited band of wave numbers. The main result thus is that the uniform state is unstable, see Fig. 7a. The dependence $c_i(k)$ is shown in

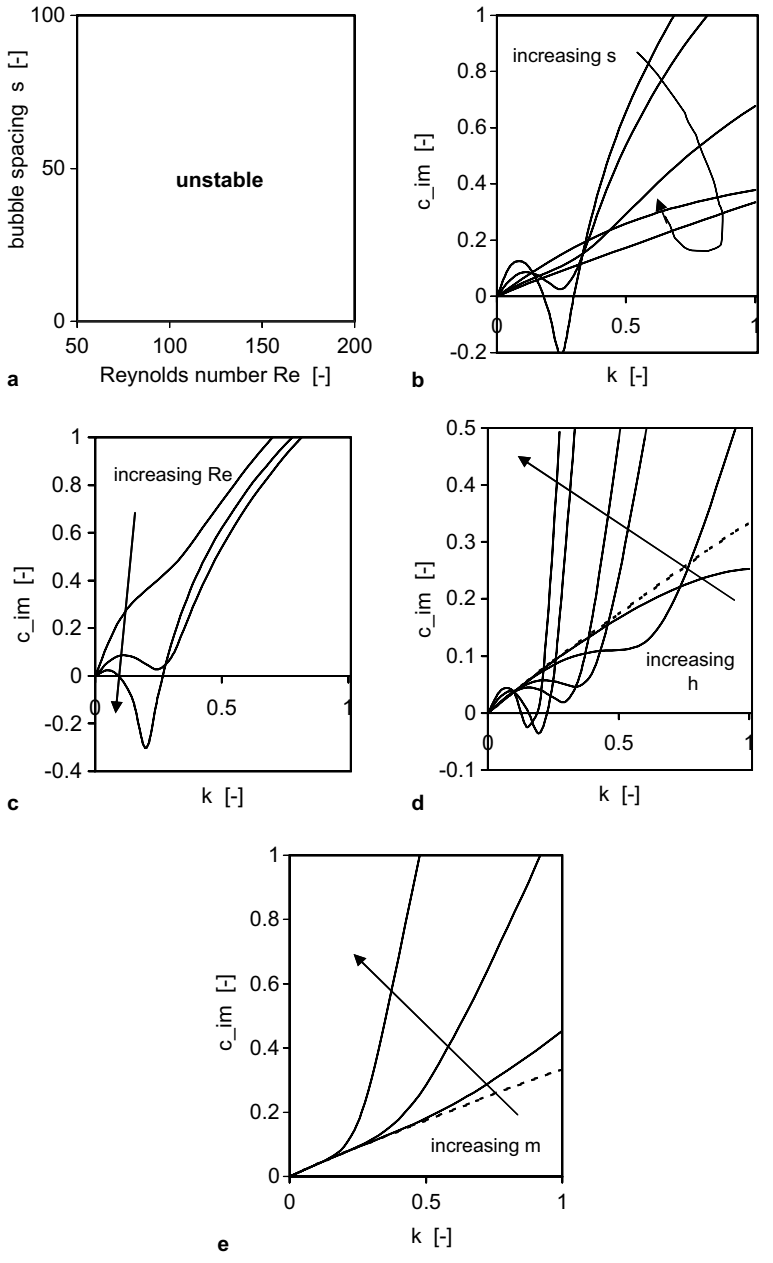

Fig. 7. Bubbly chain flow. (a) Stability diagram in parameter plane s–Re, and (b)–(e) Plot of growth factor c_i versus wave number k. Nearest-neighbour approximation ($h = m = 0$): effect of (b) bubble spacing ($s = 2.6$, 3, 5, 10, 100; $Re = 100$) and (c) Reynolds number ($s = 3$; $Re = 50$, 100, 200). Effect of distant coupling ($s = 10$; $Re = 100$); (d) viscous ($h = 0$ (dotted), 0.001, 0.01, 0.05, 0.1, 0.5, 1; $m = 0$); and (e) inviscid ($h = 0$; $m = 0$ (dotted), 0.1, 1, 10).

(Fig. 7b–e) In the nearest-neighbour approximation, a stabilizing tendency of small s and large Re is seen in Fig. 7b and c. The same tendency was found also with the discrete and continuous

chains (Figs. 3 and 10a). On the other hand, in sharp contrast with these two cases, is the fact that the distant viscous coupling can stabilize the bubbly flow. Indeed, at strong coupling, an interval of wave numbers where the growth factor is negative is seen in Fig. 7d. At the same time, however, the positive values of the growth factor are considerable larger than without the coupling. This demonstrates the ambiguous role played by the distant viscous forces in the stability, firstly encountered in Section 3.3.2. The effect of the distant inertial coupling is unambiguous: it destabilizes the flow by increasing the growth factor, see Fig. 7e. The similar effect was also found for the continuous chain see (Fig. 10f). The bubbly chain flow is more sensitive to the viscous coupling than to the inviscid one; compare values of h and m in Figs. 7d and e.

The forces responsible for the instability of the bubbly chain flow can be identified. The negativeness of c_i in (3.3.24) is ensured by a large value of k_2, which is the primary stabilizing factor generated by the drag force (coefficient A_3). The structure of the discriminator is too complicated to tell the role of the individual forces. However, substituting from (3.3.25) into (3.3.24) and rearranging yields the stability condition in a useful polynomial form:

$$P(k) \equiv b_0 + b_2k^2 + b_4k^4 + b_6k^6 + b_8k^8 < 0, \tag{3.3.27}$$

where

$$b_0 = A_1A_3^2, \quad b_2 = -(A_2A_3^2 + A_3A_4A_6), \quad b_4 = a\phi_0A_4^2 + A_3A_4A_7 - A_3A_5A_6,$$
$$b_6 = 2a\phi_0A_4A_5 + A_3A_5A_7, \quad b_8 = a\phi_0A_5^2. \tag{3.3.28}$$

At small k, $P(k) \approx b_0$ is positive so that the basic state is unstable with respect to long waves. b_0 equals $A_1A_3^2$ where A_1 is the shielding force and A_3 is the drag force. Thus the shielding instability occurs also on the macroscale. At larger k, (note that $k \leqslant k_{\max} = 1$) the positive higher terms contribute to the instability too.

4. Discussion

4.1. Stability and scales

The stability results obtained for bubble chain on the three different length scales are presented in Tables 1, 3 and 4. We can see that the stability features depend on the scale considered, despite

Table 4
Chain stability and length scales: microscale—row 1, mesoscale—row 2, macroscale—row 3

	Local			Local + Distant			
	Vis	Pot	Full	Vis	Pot	Full	
Length scale increases: ↓							
Discrete chain	u	n	s/u	u	n	s/u	1
Continuous chain	n	n	s/u	u	n	s/u	2
Bubbly chain flow	u	u	u	u/s	u	u	3

Separately are given results for nearest-neighbour approximation (Local) and for effects of distant coupling (Local + Distant), and, for forces of different origin: viscous (Vis), potential (Pot), both (Full). Legend. Stability: s—stable, u—unstable, n—neutrally stable, n/u—either n or u depending on values of s and Re.

the fact that the system under study is 'physically the same', which is a kind of paradox. The reason is that on each scale a different model for the system is employed, which is compatible with the size of the system. Different models are represented by different governing equations, whose solutions have different properties. In case of bubble chain, the stability is given by the proportion between the stabilizing and the destabilizing forces. This proportion is given by the magnitude of the force coefficients, and this magnitude depends on the scale. For instance, the coefficient at the shielding force equals $(3/4)C'$ on microscale, $(3/4)sC'$ on mesoscale, and $(3/8)s^3C'$ on macroscale, as follows from Eqs. (3.1.2), (3.2.4) and (3.3.4). This indicates that this force increases with the scale as 1, s, s^3. Each force changes according to its particular relation to the length scale. Heuristically, we can form a 'stability ratio' of the two most relevant forces, $SR =$ (drag)/(shielding), and plot it versus the scale. Fig. 8 then shows a decrease in stability with the length scale ($C/C' \rightarrow C/sC' \rightarrow C/s^3C'$). This trend corresponds to that in mechanical systems, where, put rather plainly, 'the same forces hold together still bigger and bigger piece of matter'. The actual results show a severe drop in stability at the step micro → macro, as it is evident from comparison of Figs. 3 and 7a. On the mesoscale, the stability increases, see Fig. 10a and Table 4 (row 1 versus row 2). We cannot expect the full agreement between the results and the prediction based on SR, since this ratio has only a indicative value. Also, the stability is measured by the size of the area of the stable region in the parameter plane s–Re, which is natural, but may not be completely correct. s as the discrete length scale may not be a fully relevant quantity for the continuous models.

The multiscale methodology introduced here and demonstrated in the case of bubbles in liquids applies generally to arrays of bubbles, drops, and solids. This approach is in line with the present efforts spent on respecting the variety of different length and time scales occurring in complex systems. There are several other attempts made in multiphase systems (e.g. Li and Kwauk, 2001; Hoef et al., 2004), and in particular in gas–liquid systems (e.g. Sugiyama et al., 2001; Zun, 2002; Deen et al., 2004).

This study is limited to the linear analysis of the uniform particle lattice subjected to hydrodynamic forces. However, bubble chain is a nonlinear dissipative system and displays features of the

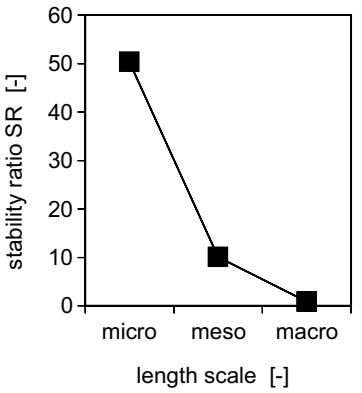

Fig. 8. Scale effect on chain stability. Stability ratio SR versus length scale. Other parameters: $s = 5$, $Re = 100$. Decreasing trend remains also for other values of s and Re.

deterministic chaos, like the corresponding mechanical analogue. Chaotic behaviour of bubble chain was demonstrate numerically in R1 and was also found in experiments (Li et al., 1997).

4.2. Stability and elasticity

We found that the wake interaction force produces the shielding instability, which is persistent with respect to the change of the length scale. The stability can be related to the elasticity property of the bubbly suspension, which is a general concept, independent of a particular configuration of the dispersed particles and value of *Re*.

4.2.1. Viscous elasticity

Microscale. The discrete shielding force D_d generates the following dynamics

$$\ddot{u}_i = -(3/4)C'(u_{i+1} - u_i) \quad (C' > 0). \tag{4.1}$$

Formally, this force is similar to 'one-half' of the elastic restoring force P_d, the half coming from the preceding neighbour,

$$\ddot{u}_i = +(3/4)C'_p(u_{i+1} - u_i) \quad (C'_p > 0). \tag{4.2}$$

As follows from (3.1.4), the physical meaning of C'_p is the spring stiffness, and its product with s is the spring modulus of elasticity, see (3.1.4). Thus, the force coefficient in (4.1) can also be interpreted in this way, saying that

$$E_1 = (3/4)sC' \tag{4.3}$$

is the microscale elasticity modulus generated by the viscous shielding ($C' = 72\,Re^{-1.5}(s-2)^{-1.6}$). The chain, as an elastic medium, supports propagation of density waves with speed

$$c_1 = (E_1/\rho_1)^{0.5}. \tag{4.4}$$

Here, the dimensionless linear density of bubble spring is $\rho_1 = 1/s$, which is m_b/d scaled by the bubble mass m_b and radius r.

Mesoscale. The continuous shielding force u_x in (3.2.4) gives the equation

$$u_{tt} = -A_{1,1}u_x \quad (A_{1,1} > 0) \tag{4.5}$$

with the dispersion relation $\omega_r = \omega_i = \pm(0.5A_{1,1}k)^{0.5}$ and the wave speed $c_2 = \omega_r/k$. The mesoscale elasticity modulus can then be defined using (4.4) as:

$$E_2 = \rho_1 c_2^2 = (3/8)C'/k. \tag{4.6}$$

Macroscale. The shielding force ϕ_x in bubbly chain flow gives

$$\phi_t + U\phi_x + \phi_0 w_x = 0, \tag{4.7}$$

$$w_t = aA_{1,1}\phi_x \quad (aA_{1,1} > 0), \tag{4.8}$$

where the growth factor $c^2 = -aA_{1,1}\phi_0$ has real $c_r = 0$ and imaginary $c_i = \pm(aA_{1,1}\phi_0)^{0.5}$ parts. The uniform state is unstable and does not support waves. If we allow for negative $(aA_{1,1})$, we obtain $c_r = \pm(aA_{1,1}\phi_0)^{0.5}$ and $c_i = 0$, which enables us to introduce the macroscale modulus

$$E_3 = \rho_m c_r^2 = 3C'(1-\phi_0)/\phi_0^2, \tag{4.9}$$

where the dimensionless gas–liquid mixture density $\rho_m \approx (1-\phi_0)$.

Now Eqs. (4.1), (4.5), (4.8) can be expressed with help of viscous elasticity:

$$\ddot{u}_i = -(E_1/s)(u_{i+1}-u_i) \quad \text{(microscale)}, \tag{4.10}$$

$$u_{tt} = -(2skE_2)u_x \quad \text{(mesoscale)}, \tag{4.11}$$

$$w_t = (E_3/\phi_0(1-\phi_0))\phi_x \quad \text{(macroscale)}. \tag{4.12}$$

All the Es are positive and the dynamics is unstable since the shielding elastic force accelerates the bubbles from sparse to dense regions. This is typical for media with negative modulus of elasticity. We can thus conclude, that the shielding instability is equivalent to the negative bulk modulus of elasticity of the bubbly mixture. The sign of the viscous force proportional to the concentration gradient depends on the sign of $\mathrm{d}C/\mathrm{d}s$, which is opposite for shielding and hindrance, see Fig. 2. For particles with hindered motion, this force term stabilizes the system.

4.2.2. Inviscid elasticity

Besides the above elasticity of viscous origin, there also is elasticity of inviscid origin, generated by the potential repulsive force. In the discrete chain, it is due to P_d, which gives (3.1.4) and the modulus

$$E_{p1} = (3/4)sC'_p \quad (C'_p = 48s^{-5}). \tag{4.13}$$

In the continuous chain, the elastic force P_d generates the term u_{xx} in the wave equation (3.2.4) with speed $c_{p2} = (A_{4,1})^{0.5}$. The corresponding modulus $\rho_1 c_{p2}^2$ then reads

$$E_{p2} = (3/4)sC'_p. \tag{4.14}$$

In the bubbly chain flow, u_{xx} turns into ϕ_{xx} in (3.3.4) and, together with the mass Eq. (3.3.3), it gives unstable basic state, $c_i = c_r = \pm(0.5aA_{4,1}k\phi_0)^{0.5}$. This demonstrates the destabilization of the potential forces in arrays when increasing the length scale, see Table 4. The corresponding modulus $\rho_m c_r^2$ becomes

$$E_{p3} = 3kC'_p(1-\phi_0)/\phi_0^3. \tag{4.15}$$

The partial dynamics corresponding to the inviscid elasticity moduli is:

$$\ddot{u}_i = (E_{p1}/s)(u_{i+1}-2u_i+u_{i-1}) \quad \text{(microscale)}, \tag{4.16}$$

$$u_{tt} = (sE_{p2})u_{xx} \quad \text{(mesoscale)}, \tag{4.17}$$

$$w_t = -(2E_{p3}/\phi_0(1-\phi_0))\phi_{xx} \quad \text{(macroscale)}, \tag{4.18}$$

where all E_ps are, again, positive. After multiplying by ρv^2, the Es becomes dimensional.

The viscous and inviscid elasticities of the chain differ in their physical origin: the former results from the dependence of the drag force on bubble spacing, while the latter from the higher pressure between vertically aligned bubbles. Both are *conservative* forces and reflect the chain resistance to the configurational changes. The former is unidirectional (wake suction) and leads to first spatial derivative. The latter is bidirectional (symmetric repulsion), which naturally leads to second spatial derivative.

4.2.3. Remark on literature

Elasticity of both kinds is also reported in the literature, mainly on fluidized bed. The viscous elasticity was employed in finding a stability criterion for uniform fluidized bed by comparing the speed of kinematic and dynamic waves, the latter being $c = (E/\rho)^{0.5}$. For instance, Verloop and Heertjes (1970) found $E = (4/3)gr(\rho_p - \rho_f)(1-\phi)$ while Foscolo and Gibilaro (1984) derived $E = 6.4\ gr(\rho_p - \rho_f)\phi$. These—and all forthcoming—formulas are written in our notation, where the voidage ϕ denotes the particle (bubble) concentration, in contrast to fluidized bed, where the particle concentration usually is $1-\phi$. The dimension of E is [N/m^2], which is [density speed^2], so the modulus scales like $\sim\rho_p v_p^2$. Both formulas were obtained heuristically, based on a simple model of a vertical line of interacting particles, with buoyancy, gravity and drag. The first modulus decreases while the second increases with particle concentration. The reason is that Verloop and Heertjes' drag decreases with spacing by the Rowe's relation (shielding), while Foscolo and Gibilaro's increases by the Richardson and Zaki's relation (hindrance).

The inviscid elasticity relates to the particle pressure p_p that generates a force $\sim -\partial p_p/\partial x = -(\partial\, p_p/\partial\phi)\phi_x$, where the coefficient is identified with the modulus, $E \equiv (\partial p_p/\partial\phi)$. Its physical origin is seen in two different sources: direct particle collisions (mechanical forces) and particle velocity fluctuations (hydrodynamic forces). The *mechanical* forces can, under certain situations, play an important role, namely in gas–solid fluidized bed. For instance, Rietema and Piepers (1990) advocate these forces arguing that there is no conservative hydrodynamic force to produce elasticity. They found $E_c = \rho_p[q_c(3-2(1-\phi_c))/(1-\phi_c)]^2$ [N/m^2], where q is the gas superficial velocity and c refers to the particular point of the homogeneous bed instability. Also, they found a general increasing dependence of E on ϕ, $E = E_0\exp(a(\phi-\phi_c))$, where $_0$ denotes a reference value. The *hydrodynamic* forces occur in any dispersed system, and are especially relevant for bubbly mixtures. The random particle fluctuations have many causes and many different manifestations, which are difficult to classify. Generally, they result from either particle–particle interactions or from particle–fluid interactions. If the motion is not much correlated, an analogy with classical thermodynamics my be helpful in providing a guideline for introducing particle 'temperature' and 'pressure'. There is an obvious anisotropy due to gravity. Since the particle fluctuations is difficult to measure or find theoretically, the closures can be obtained by simulations. If the motion displays certain coherent features, important collective phenomena may emerge on the macroscale, namely the hydrodynamic particle diffusion. Various heuristic formulas are used for the particle pressure due to hydrodynamic forces, e.g. $p_p \sim \phi$ or $\sim\phi/(\phi_{\max}-\phi)$, to reflect the expected increase with the concentration. The corresponding moduli are ~const. or increasing with ϕ.

4.3. Macroscale equations

Soon it was recognized that a force proportional to the concentration gradient ϕ_x can stabilize the uniform basic state of macroscopic governing equations. Such force term was introduced purely *formally*, for particles in general positions, because it was beneficial for the system stability. It comes from the divergence of the particle stress tensor, namely from the normal stresses (particle pressure). The term $w_t \sim -E\phi_x$ represents a force due to the expected resistance of the mixture to configurational changes. The degree of the mixture 'deformation' or 'compression' is expressed by ϕ_x . When $E > 0$, the force tends to smear out concentration gradients by pushing

the particles from dense to diluted regions, hence stabilizes the uniform state—compare with (4.12).

The gradient terms are also obtained by a great variety of *averaging methods*. They differ in many aspects (average of what over what, assumptions necessary for the statistics, assumptions about the flow field, formulation of particle interactions, etc.) and face the very fundamental problems of multiphase mechanics. All basically are a one-step process, micro → macro. A 'meso-scale' parcel of the mixture can be considered to have statistically homogeneous sample to define the constant mean. These efforts present the main stream in developing the governing bubbly equations.

The macroscopic governing equations can also be obtained from *physical considerations* on the microscale, taking into account those processes involved in the momentum transfer that are currently known and seem relevant. Here, the terms with ϕ_x are related to specific physical mechanisms. As an example of such equations, we present those by Batchelor (1988):

$$\phi_t + U\phi_x + \phi_0 w_x = 0 \quad \text{(mass)}, \tag{4.19}$$

$$p_1(w_t + w_x) = p_2 w_x + p_3 w_{xx} - p_4\phi_x + (1/Fr^2)(p_5\phi - p_6 w - p_7\phi_x) \quad \text{(momentum)}. \tag{4.20}$$

They are dimensionless, written for small disturbances in 1D flow, for particles in general positions undergoing both *vertical* and *horizontal* interactions that results in the hindrance effect. The reference frame travels with the mean mixture velocity and with the axis pointing downward.

These should be compared with (3.3.3) and (3.3.4) obtained here for the bubbly chain flow, with the *vertical* interactions only, with the typical shielding effect, that in the nearest-neighbour approximation read:

$$\phi_t + U\phi_x + \phi_0 w_x = 0 \quad \text{(mass)}, \tag{4.21}$$

$$w_t = (1/Re)(q_1\phi_x - q_2 w) - q_3\phi_{xx} - q_4 w_x \quad \text{(momentum)}. \tag{4.22}$$

In (4.20), the terms with the Froude number are noninertial and long-range, while the other are inertial and short-range. There are two terms related to the elasticity of either origin. Term—$p_4\phi_x$ represents the normal stress due to particles velocity fluctuations, and term—$(1/Fr^2)p_7\phi_x$ corresponds to the hydrodynamic diffusion. Both stabilize the uniform state provided that the coefficients p_4 and p_7 are positive. The expression for these two are based on scale estimates. In (4.22), the terms with the Reynolds number are viscous and long-range, while the other are inviscid and short-range. There also are two elastic terms of either origin. Term $+(1/Re)q_1\phi_x$ is the viscous shielding and $-q_3\phi_{xx}$ the inviscid repulsion. Both destabilize the system. The coefficients are positive and expressed rigorously.

Besides the elasticity, both Eqs. (4.20) and (4.22), also have acceleration, w_t, w_x, and drag, w. On the other hand, (4.20) has buoyancy ϕ and particle viscosity w_{xx}. The buoyancy is not in (4.22) because of the choice of the reference frame. The term w_{xx} reflects the conformational resistance due to shear stresses in the fluid, not considered in (4.22), where the bubbles move through a stagnant liquid.

Although the model (4.20) is based on a detailed list of relevant physical processes, it is very difficult to state clearly and unequivocally whether the list is complete, which of them are independent, which interfere and to what extent, and how the closure formulas should look like. This is quite apparent when reading the Batchelor's paper. In this context, certain comparative

advantages of the approach presented in this study can be seen. It is relatively easy to follow the changes of the few basic forces when moving from micro to macro scale. No statistics is needed, since the averaging procedures are avoided. It will work also for 2D and 3D cases, once we correctly know the particle interaction forces at the leading order. Efforts in this respect are currently under way.

Note that considering the distant coupling results in higher spatial derivatives, which formally could appear in previous derivations, but their physical content was not substantiated. Now we have a physical mechanism that causes dispersion, and, consequently, could lead to voidage solitary waves, which, unlike in fluidized beds, have not been observed in bubbly flows. It could happen when the vertical interactions will be able to produce certain level of dynamic coherency on longer spatial scales. Let us hunt for bubbly solitons!

Acknowledgments

The author highly appreciates the long-term intellectual contact with his hydrodynamic guru, Neale Hillyer Thomas, FRED Ltd., Birmingham, UK (formerly at DAMTP). This work benefited from the author's working visit at the Department of Applied Mathematics and Theoretical Physics (DAMTP), University of Cambridge, Cambridge, UK, thanks to Prof. H.E. Huppert and Prof. N.H. Thomas. The support by the GACR (no. 104/04/0827) and by the EC (BEMUSAC Project No. G1MA-CT-2002- 04019) is gratefully acknowledged. Some aspects of the present work have been announced at the 5th EUROMECH Fluid Mechanics Conference (Toulouse, France, 2003), 5th International Conference on Multiphase Flow (Yokohama, Japan, 2004), and 42nd European Two Phase Flow Group Meeting (Genova, Italy, 2004).

Appendix A. Stability of mesoscale model

The mesoscale momentum equation (3.2.4) contains seven coefficients of different origin:

$$
\begin{aligned}
A_1 &= (D_d + V_d) = 0.75s[C' + h(2C_2^{*\prime} + 3C_3^{*\prime} + 4C_4^{*\prime})] \sim Re^{-1.5}(s^{-0.6} + \exp(-s/Re)),\\
A_2 &= (V_d) = hs^3(3.37C_3^{*\prime} + 8C_4^{*\prime}) \sim s^3 Re^{-1.5}\exp(-s/Re),\\
A_3 &= (D_v + V_v) = 1.5(C - hC^*) \sim (Re^{-1} - Re^{-1.5}) - s^{-0.6}Re^{-1.5},\\
A_4 &= (P_d + LR_d + V_d) = s^2[0.75C_p' + 0.133mC_p' - h(1.5C_2^{*\prime} + 3.37C_3^{*\prime} + 6C_4^{*\prime})] \sim s^{-3} - s^2 Re^{-1.5}\exp(-s/Re),\\
A_5 &= (LR_d + V_d) = s^4(0.067m\,C_p' - 8hC_4^{*\prime}) \sim s^{-1} - s^4 Re^{-1.5}\exp(-s/Re),\\
A_6 &= (P_v + LR_v) = sC_p(3 + 0.532m) \sim s^{-3},\\
A_7 &= (LR_v) = 0.541ms^3 C_p \sim s^{-1},
\end{aligned}
\tag{A.1}
$$

The discrete source-forces of the coefficients are indicated in the parenthesis—they determine the physical content of the As, see Table 3. The coefficients A_2, A_5 and A_7 are produced by the distant forces and are linear in h and m. The other involve both local ($A_{1,1}, A_{3,1}, A_{4,1}, A_{6,1}$) and distant ($A_{1,2}, A_{3,2}, A_{4,2+3}, A_{6,2}$) contributions. Here, $A_{n,k}$ denotes the kth summand in A_n and all these summands are positive and correspond to the individual source-forces. Also, $A_{n,k+m}$ denotes

$A_{n,k} + A_{n,m}$. A_1–A_3 are purely viscous and decrease with increasing Re. A_6–A_7 are purely inviscid and independent of Re. A_4 and A_5 are of a mixed origin: $A_{4,1+2}$ and $A_{5,1}$ are inviscid and $A_{4,3}$ and $A_{5,2}$ are viscous. The coefficients A_1–A_3, A_6 and A_7 are positive; A_3 must be to keep its physical meaning. A_4 and A_5 can be negative at strong viscous coupling. The typical magnitude of the coefficients is 10^{-2}–10^{0} and depends strongly on the parameters s and Re, as indicated in Eq. (A.1). With increasing s, all coefficients but A_3 (total drag) tend to zero asymptotically. Only A_1, A_6 and A_7 fall monotonously. A_2 goes through a maximum, while A_4 and A_5 go through a minimum. A_3 rises with s and saturates at the value of the single bubble drag. The viscous coupling h influences the coefficients strongly and is more important than the inviscid coupling m. The relative magnitude of the coefficients is important for the chain behaviour. The viscous terms (long-range and Re-dependent) can be separated from the inviscid terms (short-range and Re-independent) by either decreasing Re or increasing s.

The stability of the basic state, the uniform spacing $u(x,t) \equiv 0$, is tested by inserting the wave solution $\sim\exp[\mathrm{i}(kx - \omega_t)]$ into the governing equation (3.2.4), which gives the dispersion relation:

$$-\omega^2 = -A_1 k\mathrm{i} + A_2 k^3\mathrm{i} + A_3\omega\mathrm{i} - A_4 k^2 + A_5 k^4 - A_6\omega k + A_7\omega k^3. \tag{A.2}$$

The stability features of the individual terms in (3.2.4) are shown in Table 3.

Viscous waves: When the viscous forces dominate, (3.2.4) reduces to

$$0 = -A_1 u_x - A_2 u_{xxx} - A_3 u_t - A_{4,3} u_{xx} \tag{A.3}$$

and the dispersion equation

$$0 = -A_1 k\mathrm{i} + A_2 k^3\mathrm{i} + A_3\omega\mathrm{i} + A_{4,3} k^2 \tag{A.4}$$

gives

$$\omega_r = (A_1/A_3)k - (A_2/A_3)k^3, \tag{A.5}$$

$$\omega_i = (A_{4,3}/A_3)k^2 \geqslant 0. \tag{A.6}$$

In the nearest-neighbour approximation ($A_2, A_{4,3} = 0$), $\omega_i = 0$ and the uniform state is *neutrally stable*, for the first time with the viscous forces. The viscous waves $u_t + (A_{1,1}/A_{3,1})u_x = 0$ propagate freely at the speed $c = (A_{1,1}/A_{3,1}) \sim$ (local shielding/drag). These are the continuity waves with which the viscous dissipation, as a dynamical process, does not interfere. With the distant forces, $\omega_i > 0$ and the chain is unstable due to the viscous coupling $A_{4,3} \sim$ (distant shielding). The other distant term, A_2, causes the normal dispersion in ω_r.

Inviscid waves: When the inviscid forces dominate, (3.2.4) reduces to

$$u_{tt} = A_{4,1+2} u_{xx} + A_{5,1} u_{xxxx} - A_6 u_{tx} - A_7 u_{txxx}, \tag{A.7}$$

which gives the dispersion relation with $\omega_i = 0$. The uniform state is thus neutrally stable and supports inviscid waves. The real part, responsible for dispersion, obeys

$$-\omega_r^2 = -A_{4,1+2} k^2 + A_{5,1} k^4 - A_6\omega_r k + A_7\omega_r k^3. \tag{A.8}$$

In the nearest-neighbour approximation, the frequency is

$$\omega_r = (1/2)k(A_{6,1} \pm (A_{6,1}^2 + 4A_{4,1}))^{0.5} \tag{A.9}$$

and the waves propagate without dispersion. The distance-related force (P_d) itself recovers the standard wave equation $u_{tt} = A_{4,1}u_{xx}$ with two modes $\omega_r = \pm(A_{4,1})^{0.5}k$. The velocity-related force (P_v) gives the equation $u_{tt} = -A_{6,1}u_{tx}$ with only one mode $\omega_r = A_{6,1}k$.

The distant coupling causes the normal dispersion by the higher spatial derivatives. The distance-related force ($P_d + mLR_d$) has

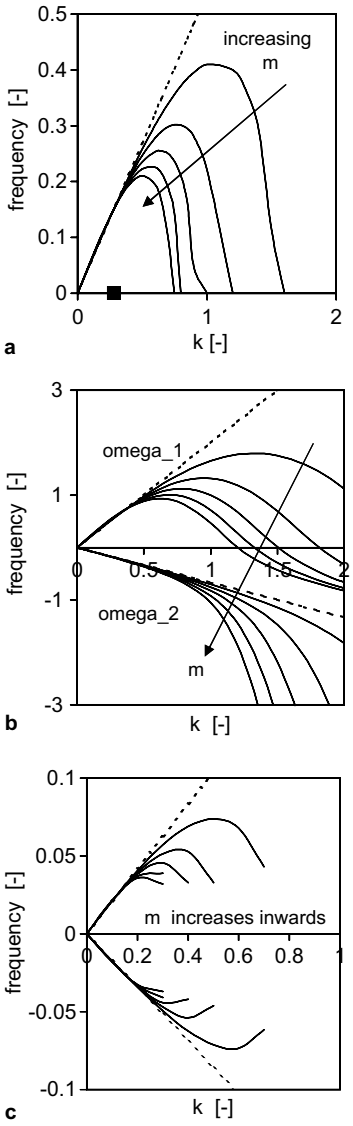

Fig. 9. Continuous chain. Effect of inertial coupling m on inviscid waves. (a) Dispersion relation (A9) ($s = 5$). Black square: $k_c = 0.28$ at $m \to \infty$. Dispersion relation (A11) at (b) low bubble spacing ($s = 3$) and (c) high bubble spacing ($s = 10$). Parameter $m = 0$ (dotted lines), 0.2, 0.4, 0.6, 0.8, 1. Other parameters: $h = 0$, $p = q = 3$. Note anomalous dispersion of ω_2 in (b).

$$\omega_r = \pm k(A_{4,1+2} - A_{5,1}k^2)^{0.5}. \tag{A.10}$$

The waves can propagate for $k < k_c = (A_{4,1+2}/A_{5,1})^{0.5} = s^{-1}(1.98 + 11.1/m)^{0.5}$, where ω_r is real and nonzero. The value of k_c decreases with the coupling strength m, see Fig. 9a. At zero coupling ($m = 0$), k_c is infinite and the spectrum is not limited from above. There is, however, a physical limit on k given by the scaling: the wave cannot be shorter than the bubble size, so that the dimensionless k must be smaller than $k_{\max} \sim O(1)$. At the extreme coupling ($m \to \infty$), $k_c \approx 1.4/s$ and the wavelength must be larger then $\lambda_c = 2\pi/k_c \approx 4.45s$. Beyond k_c, ω_r would be complex, which is not allowed. The velocity-related force ($P_v + mLR_v$) gives one mode

$$\omega_r = k(A_6 - A_7k^2) \tag{A.11}$$

and the spectrum is limited by $k_c = (A_6/A_7)^{0.5} = s^{-1}(0.983 + 5.54/m)^{0.5}$. At the extreme coupling, it gives $\lambda_c \approx 6.33s$.

Eq. (A.7) of the total inviscid force has two branches of solution

$$\omega_{r,1,2} = (1/2)(A_6k - A_7k^3 \pm \sqrt{\mathrm{Dis}}), \quad \mathrm{Dis} = (-A_6k + A_7k^3)^2 + 4(A_{4,1+2}k^2 - A_{5,1}k^4), \tag{A.12}$$

that differ slightly at lower spacing and become $\pm$ symmetric at higher spacing, see Figs. 9b and c.

Stability of continuous chain: The full dispersion relation (A.2) yields a quartic equation for the imaginary part

$$c_0 + c_1\omega_i + c_2\omega_i^2 + c_3\omega_i^3 + c_4\omega_i^4 = 0, \tag{A.13}$$

where the coefficients are

$$\begin{aligned}
c_0 &= (-A_1^2 + A_3^2A_4 + A_1A_3A_6)k^2 + (2A_1A_2 - A_3^2A_5 - A_2A_3A_6 - A_1A_3A_7)k^4 + (-A_2^2 + A_2A_3A_7)k^6,\\
c_1 &= A_3^3 + (4A_3A_4 + A_3A_6^2)k^2 - (4A_3A_5 + 2A_3A_6A_7)k^4 + A_3A_7^2k^6,\\
c_2 &= 5A_3^2 + (4A_4 + A_6^2)k^2 - (4A_5 + 2A_6A_7)k^4 + A_7^2k^6,\\
c_3 &= 8A_3,\\
c_4 &= 4.
\end{aligned} \tag{A.14}$$

The uniform state is stable when $\omega_i(k, s, Re, h, m) < 0$, i.e. for all $k \leqslant k_{\max} = 1$. Typically, the first root of (A.12) is negative, the other two are either real negative or complex (unphysical), and the stability decisive fourth root is either negative or positive, depending on the parameters. The final result is in Fig. 10a, where the parameter plane s–Re is divided into the stable and unstable regions. The main source of the instability is the shielding force, accelerating the bubbles from sparse to dense regions, $u_{tt} \sim -u_x$. Qualitatively, Fig. 10a is similar to Fig. 3 for the discrete chain: the stable region occurs at low s and high Re and is considerably reduced by the distant coupling. On the other hand, the numerical values of the critical spacing in Fig. 10a are by one order larger comparing with Fig. 3. The fourth root is plotted in Fig. 10b–f. In the nearest-neighbour approximation, the destabilizing effect of the spacing is demonstrated in Fig. 10b. The lines start in the origin and fall or rise monotonously. The instability due to the viscous coupling occurs at long waves, as shown in Fig. 10c and d. In contrast, the instability due to the inertial coupling begins at short waves, as shown in Fig. 10e and f. This reflects the difference between the long- and short-range character of the viscous and inviscid forces. The chain is relatively sensitive to both

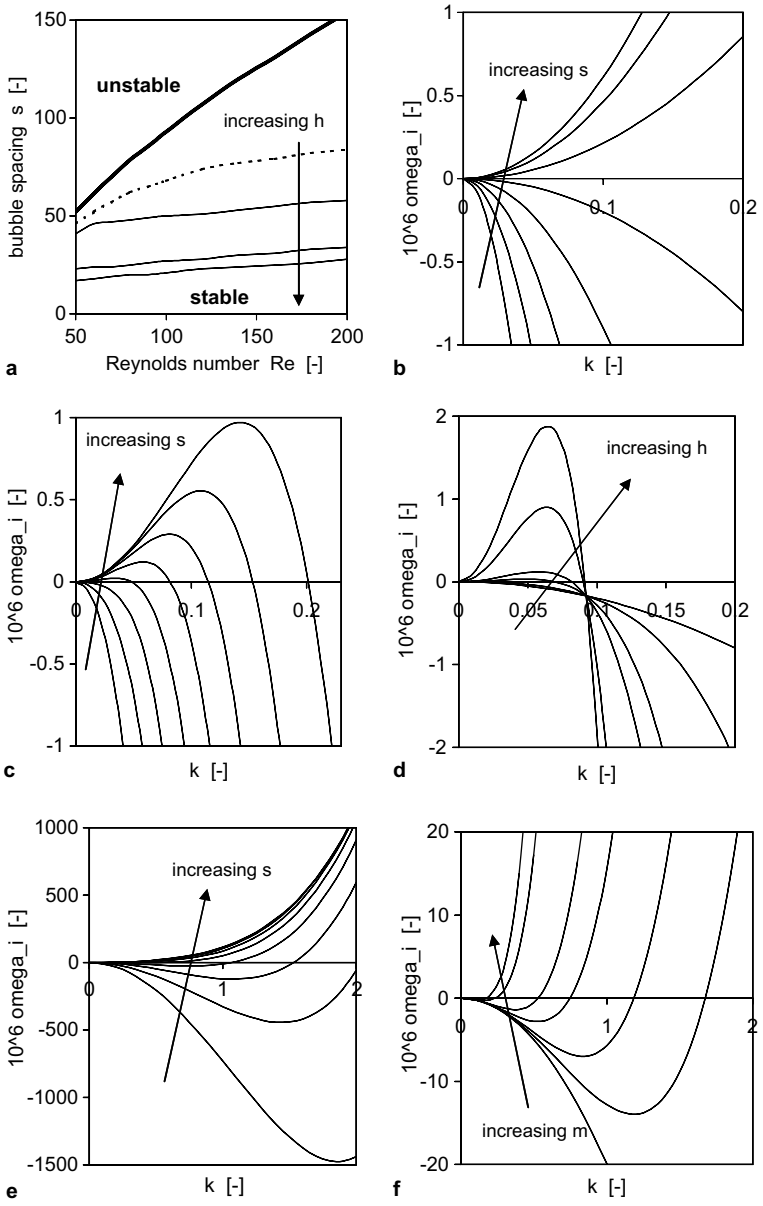

Fig. 10. Continuous chain. (a) Stability diagram in parameter plane s–Re. Bold line: local forces ($h = m = 0$). Thin lines: effect of viscous distant forces ($h = 0.001,\ 0.005,\ 0.01$; $m = 0$). Dotted line: effect of inviscid distant forces ($h = 0, m = 0.001$). Other parameters: $Re = 100$, $p = q = 3$. (b)–(f) Imaginary part of frequency ω_i versus wave number k. (b) Nearest-neighbour approximation: effect of bubble spacing ($h = m = 0$). (c) Viscous distant coupling considered: effect of bubble spacing ($h = 0.001$, $m = 0$). (d) Viscous distant coupling considered: effect of coupling strength ($h = 0$, 0.0001, 0.0005, 0.001, 0.005, 0.01; $m = 0$; $s = 50$). (e) Inviscid distant coupling considered: effect of bubble spacing ($h = 0, m = 0.001$). (f) Inviscid distant coupling considered: effect of coupling strength ($h = 0$; $m = 0$, 0.0001, 0.0002, 0.0005, 0.001, 0.005, 0.01; $s = 50$). In (b, c, e): $s = 30$, 35, 40, 45, 50, 55, 60, 65. Other parameters: $Re = 50$, $p = q = 3$.

the viscous and inviscid couplings and even small values of h and m produce considerable effects. Unlike with the discrete chain, where the viscous effects were much stronger, the impacts of both couplings are comparable at the continuous chain (c.f. Fig. 10d and f). The full chain cannot support waves because ω_i is typically nonzero. The rare exception is the vicinity of the critical lines in Fig. 10a, where $\omega_i = 0$ at some value of k. Also, in the long wave limit $k = 0$, the value $\omega_i = 0$ solves (A.12).

Despite the fact that the mesoscale concept (single string after the continuum limit) may look somewhat artificial, the stability analysis of the continuous chain gives valuable information about the underlying processes. Similar investigation has been done for granular flows, where both linear and nonlinear waves are studied theoretically for a continuous chain of particles (Hinch and Saint-Jean, 1999). Likely, the first mesoscale treatment of gas–liquid systems is done in the present study. On the experimental side, one needs a long enough chain to consider it truly continuous, as mentioned in Section 3.2. Another way to the continuity leads via bubbles that are connected to one another, which can occur e.g. in polymeric liquids (Kliakhandler, 2002). Conceptually, the meso-scale concept is not dissimilar to what is called 'intermediate asymptotics' (Barenblatt, 1996): "...The analogy with painting is made: we stand far enough back for the brush strokes to be invisible, but close enough to appreciate the art...".

References

Barenblatt, G.I., 1996. Scaling, Self-similarity, and Intermediate Asymptotics. Cambridge University Press, Cambridge, UK.

Batchelor, G.K., 1988. A new theory of the instability of a uniform fluidized bed. J. Fluid Mech. 193, 75–110.

Bernasconi, J., Schneider, T., 1981. Physics in One Dimension. Springer, Berlin.

Broadhurst, T.E., 1986. Particle oscillation in fluidized beds. In: Cheremisinoff, N.P. (Ed.), Encyclopedia of Fluid Mechanics, vol. 4. Gulf Publishing Company, Houston, pp. 781–815.

Cai, X., Wallis, G.B., 1992. Potential flow around a row of spheres in a circular tube. Phys. Fluids A4, 904–912.

Coppock, P.D., Meiklejohn, G.T., 1951. The behaviour of gas bubbles in relation to mass transfer. Trans. Instn. Chem. Engrs. 29, 75–86.

Deen, N.G., van Sint Annaland, M., Kuipers, J.A.M., 2004. Multi-scale modeling of dispersed gas–liquid two-phase flow. Chem. Eng. Sci. 59, 1853–1861.

Dixon, D.C., Souter, P., Buchanan, J.E., 1976. A study of inertial effects in sedimentation. Chem. Eng. Sci. 31, 737–740.

Foscolo, P.U., Gibilaro, L.G., 1984. A fully predictive criterion for the transition between particulate and aggregate fluidization. Chem. Eng. Sci. 39, 1667–1675.

Galper, A.R., Miloh, T., 1998. Motion stability of a deformable body in an ideal fluid with applications to the N spheres problem. Phys. Fluids 10, 119–130.

Happel, J., Brenner, H., 1965. Low Reynolds Number Hydrodynamics. Prentice-Hall, Englewood Cliffs, NJ.

Harper, J.F., 1970. On bubbles rising in line at large Reynolds number. J. Fluid Mech. 41, 751–758.

Harper, J.F., 1997. Bubbles rising in line: why is the first approximation so bad? J. Fluid Mech. 351 289–300.

Harper, J.F., 2001. Growing bubbles rising in line. J. App. Maths. Decision Sci. 5, 65–73.

Hinch, E.J., Saint-Jean, S., 1999. The fragmentation of a line of balls by an impact. Proc. Roy. Soc. Lond. A 455, 3201–3220.

Hirose, A., Lonngren, K.E., 1985. Introduction to Wave Phenomena. Wiley, New York.

Hoef, M.A.van der, van Sint Annaland, M., Kuipers, J.A.M., 2004. Computational fluid dynamics for dense gas–solid fluidized beds: a multi-scale modeling strategy. Chem. Eng. Sci. 59, 5157–5165.

Katz, J., Meneveau, C., 1996. Wake-induced relative motion of bubbles rising in line. Int. J. Multiphase Flow 22, 239–258.
Kliakhandler, I.L., 2002. Continuous chain of bubbles in concentrated polymeric solutions. Phys. Fluids 14, 3375–3379.
Lamb, H., 1932. Hydrodynamics. Cambridge University Press, Cambridge.
Lerner, L., Harper, J.F., 1991. Stokes flow past a pair of stagnant-cap bubbles. J. Fluid Mech. 232, 167–190.
Li, H.Z., Mouline, Y., Choplin, L., Midoux, N., 1997. Chaotic bubble coalescence in non-Newtonian fluids. Int. J. Multiphase Flow 23, 713–723.
Li, J., Kwauk, M., 2001. Multiscale nature of complex fluid-particle systems. Ind. Eng. Chem. Res. 40, 4227–4237.
Liger-Belair, G., Jeandet, P., 2002. Effervescence in a glass of champagne: A bubble story. Europhys. News 33 (1), 10–14.
Magnaudet, J., Eames, I., 2000. The motion of high-Reynolds-number bubbles in inhomogeneous flows. Ann. Rev. Fluid Mech. 32, 659–708.
Main, I.C., 1984. Vibrations and Waves in Physics, second ed. Cambridge University Press, Cambridge.
Manasseh, R., Nikolovska, A., Ooi, A., Yoshida, S., 2004. Anisotropy in the sound field generated by a bubble chain. J. Sound Vibr. 278, 807–823.
Mattis, D.C., 1993. The Many-body Problem. An Encyclopedia of Exactly Solved Models in One Dimension, second ed. World Scientific, Singapore.
Miyahara, T., Kaseno, S., Takahashi, T., 1984. Studies on chains of bubbles rising through quiescent liquid. Can. J. Chem. Eng. 62, 186–193.
Moore, D.W., 1963. The boundary layer on a spherical gas bubble. J. Fluid Mech. 16, 161–176.
de Nevers, N., Wu, J.L., 1971. Bubble coalescence in viscous fluids. AIChE J. 17, 182–186.
Pruppacher, H.R., Klett, J.D., 1998. Microphysics of Clouds and Precipitation, second ed. Kluwer, Dordrecht.
Richardson, J.F., Zaki, W.N., 1954. Sedimentation and fluidization: Part I. Trans. Instn. Chem. Engrs. 32, 35–53.
Rietema, K., Piepers, H.W., 1990. The effect of interparticle forces on the stability of gas-fluidized beds—I. Experimental evidence. Chem. Eng. Sci. 45, 1627–1639.
Ruzicka, M.C., 2000. On bubbles rising in line. Int. J. Multiphase Flow 26, 1141–1181, denoted R1.
Sanada, T., 2005. Interaction and Coalescence of Bubbles in Quiescent Liquid. Ph.D. Thesis, Graduate School of Engineering, Kyushu University, Fukuoka, Japan.
Sankaranaranayan, K., Shan, X., Kevrekidis, I.G., Sundaresan, S., 2002. Analysis of drag and virtual mass forces in bubbly suspensions using an implicit formulation of the lattice Boltzmann method. J. Fluid Mech. 452, 61–96.
Sirignano, W.A., 1999. Fluid Dynamics and Transport of Droplets and Sprays. Cambridge University Press.
Sonshine, R.M., Brenner, H., 1966. The Stokes translation of two or more particles along the axis of an infinitely long circular cylinder. Appl. Sci. Res. 16, 425–454.
Sugiyama, K., Takagi, S., Matsumoto, Y., 2001. Multi-scale analysis of bubbly flows. Comput. Meth. Appl. Mech. Eng. 191, 689–704.
Verloop, J., Heertjes, P.M., 1970. Shock waves as a criterion for the transition from homogeneous to heterogeneous fluidization. Chem. Eng. Sci. 25, 825–832.
Voinov, O.V., 2001. Motion stability of a periodic system of bubbles in a liquid. J. Fluid Mech. 438, 247–275.
de Vries, A.W.G., Biesheuvel, A., van Wijngaarden, L., 2002. Notes on path and wake of a gas bubble rising in pure water. Int. J. Multiphase Flow 28, 1823–1835.
Werther, J., 1977. Bubble chains in large diameter gas fluidized beds. Int. J. Multiphase Flow 3, 367–381.
Wolfram, S., 1999. The Mathematica Book, fourth ed. Cambridge University Press, New York.
Yuan, H., Prosperetti, A., 1994. On the in-line motion of two spherical bubbles in a viscous fluid. J. Fluid Mech. 278, 325–349.
Zhang, J., Fan, L.S., 2003. On rise velocity of an interactive bubble in liquids. Chem. Eng. J. 92, 169–176.
Zun, I., 2002. Phase discrimination vs. multiscale characteristics in bubbly flow. Exp. Thermal Fluid Sci. 26, 361–374.